Stem Cell Research & Therapy

RESEARCH

Open Access

RNA-binding protein SAMD4A targets FGF2 to regulate cardiomyocyte lineage specification from human embryonic stem cells

Na Yi[1,2,3†], Han-rui Wang[1,2,3†], Yu-ping Zhu[1,2,3], Tao Xiao[1,2,3], Qin Lin[1,2,3], Huan Liu[1,2,3], Yi-lei Meng[1,2,3], Yi-zhuo Sun[1,2,3], Fang Lin[1,2,3], Sang-yu Hu[1,2,3], Hua-ming Cao[4], Jun-fang Zhang[1], Lu-ying Peng[1,2,3*] and Li Li[1,2,3*]

Abstract

Background RNA-binding proteins (RBPs) are essential in cardiac development. However, a large of them have not been characterized during the process.

Methods We applied the human embryonic stem cells (hESCs) differentiated into cardiomyocytes model and constructed *SAMD4A*-knockdown/overexpression hESCs to investigate the role of SAMD4A in cardiomyocyte lineage specification.

Results SAMD4A, an RBP, exhibits increased expression during early heart development. Suppression of SAMD4A inhibits the proliferation of hESCs, impedes cardiac mesoderm differentiation, and impairs the function of hESC-derived cardiomyocytes. Correspondingly, forced expression of SAMD4A enhances proliferation and promotes cardiomyogenesis. Mechanistically, SAMD4A specifically binds to *FGF2* via a specific CNGG/CNGGN motif, stabilizing its mRNA and enhancing translation, thereby upregulating FGF2 expression, which subsequently modulates the AKT signaling pathway and regulates cardiomyocyte lineage differentiation. Additionally, supplementation of FGF2 can rescue the proliferation defect of hESCs in the absence of SAMD4A.

Conclusions Our study demonstrates that SAMD4A orchestrates cardiomyocyte lineage commitment through the post-transcriptional regulation of FGF2 and modulation of AKT signaling. These findings not only underscore the essential role of SAMD4A in cardiac organogenesis, but also provide critical insights into the molecular mechanisms underlying heart development, thereby informing potential therapeutic strategies for congenital heart disease.

Keywords RNA-binding protein, SAMD4A, Cardiomyocyte differentiation, FGF2, FGFR2, Stem cell

†Na Yi and Han-rui Wang contributed equally to this work.

*Correspondence:
Lu-ying Peng
luyingpeng@tongji.edu.cn
Li Li
lilirz@tongji.edu.cn

[1]State Key Laboratory of Cardiovascular Diseases and Medical Innovation Center, Shanghai East Hospital, School of Medicine, Tongji University, Shanghai 200120, China
[2]Shanghai Arrhythmias Research Center, Shanghai East Hospital, Tongji University School of Medicine, Shanghai 200120, China
[3]Stem Cell Research Center, Medical School, Tongji University, Shanghai 200120, China
[4]Department of Cardiology, Shanghai Shibei Hospital, Shanghai 200435, China

Background

The heart is the earliest functional organ formed during embryonic development governed by complex regulatory process, including signaling pathways, transcription factors (TF), epigenetic factors [1–3], and post-transcriptional regulators [4]. Many mutants of crucial genes have been identified to be involved in congenital heart disease (CHD) [5, 6], which represents the most prevalent birth defect with an estimated prevalence of 1% live births globally [7]. Epidemiological studies reveal that surgical interventions are mandated for 25% of diagnosed cases during infancy [8]. Despite remarkable progress in perinatal care, CHD remains the leading cause of mortality among pediatric patients with congenital disorders [9]. However, the multifactorial pathogenesis of CHD remains incompletely understood.

Recent advances highlight the underappreciated role of RBPs in orchestrating cardiac development, encompassing cardiac tube development, heart formation, and the process of developmental maturation [10]. Concurrently, numerous studies have elucidated that RBPs are crucial in post-transcriptional regulation processes, thereby influencing the pluripotency of stem cell, and guiding differentiation through various pathways [11]. Additionally, RBPs are involved in the regulation of alternative splicing [12–14], alternative polyadenylation [15], RNA modification [16], and transcript export [17]. These proteins also govern the translation process by binding to the 5'UTR [18] involved in mRNA stability [19]. For example, the RBP Lin28 inhibits the process of pri-let-7 miRNA processing in embryonic stem cells (ESCs), showing a crucial mechanism in early embryonic development and somatic cell reprogramming [20]. Lin28 also promotes cardiomyocyte proliferation in the injured heart [21]. Moreover, the RBP QKI is highly expressed in the heart, and governs the pre-mRNA alternative splicing for the genes associated with Z-disk formation and cardiomyocyte contractile function. This regulatory role is indispensable of both cardiomyogenesis and the maintenance of cardiomyocyte contractile function [22, 23]. *RBFOX2* mutations are linked to functional defects and are closely associated with hypoplastic left heart syndrome (HLHS). Knockout-*Rbfox2* mice developed severe defects in embryonic heart development. RBFOX2 oversees the alternative splicing of the genes associated with the endocardial-mesenchymal transition, a critical process in cardiac development [24].

Although RBPs are essential for normal heart development, the functions of most RBPs and their targets during cardiomyocyte differentiation remain enigmatic. Our previous study revealed an increase pattern of SAMD4A as an RBP during the differentiation of both hESCs and murine ESCs (mESCs) into cardiomyocytes [25]. In human heart, SAMD4A is specifically expressed in ventricular cardiomyocytes [26]. In addition, SAMD4A expression is significantly decreased in CHD [27]. The mammalian SAMD4A features a sterile alpha motif (SAM) that binds to RNA stem-loop structures named Smaug protein recognition elements (SREs), which target mRNAs with consensus sequences CNGG or CNGGN [28]. Smaug can recruit proteins such as CUBP1 [29]. (CUG triplet repeat RNA-binding protein 1) and Argonaute1 [30] that degrade the targeted mRNAs, thus impeding Drosophila early embryonic development [31–33]. Furthermore, *Samd4* mutant mice exhibited leanness, myopathy, and impaired mitochondrial respiratory coupling, with metabolic impairments tightly coupled to the disruption of mTORC1 signaling pathways, essential for cellular growth and metabolic integrity [34]. *Samd4* knockout mice also displayed deferred bone development and decreased osteogenesis by binding to *Mig6* mRNA and inhibiting the synthesis of MIG6 protein [35]. Collectively, these evidences highlight the pivotal role of SAMD4A in various developmental processes. However, its cardiogenic functions and mechanistic underpinnings remain completely unexplored.

Hence, we explored the involvement of SAMD4A in the cardiomyogenesis process using the hESC-induced cardiomyocyte differentiation model. Our findings reveal that SAMD4A knockdown impedes hESCs proliferation and hinders cardiomyogenesis, while overexpression of SAMD4A in hESCs promotes cardiomyocyte differentiation. Additionally, we demonstrated that SAMD4A is involved in regulating the PI3K/AKT/mTOR signaling pathways through its association with *FGF2*, influencing stem cell proliferation and lineage differentiation. This study elucidates the pivotal regulatory function of SAMD4A in determining stem cell fate and specifying the cardiomyocyte lineage, providing critical insights into the mechanisms underlying CHD pathogenesis.

Materials and methods

Human embryonic stem cell culture

Human ESC line WA07 (H7) used in this study was kindly donated by Prof. Qing Jing from Shanghai Institutes for Biological Sciences Chinese Academy of Sciences. For a monolayer-based culture, human ESC H7 was cultured on Matrigel-coated plates (Cat#354277, Corning, New York, NY, USA) within mTeSR™ Plus medium (Cat#100–0276, STEMCELL Technologies, Vancouver, Canada) and medium was needed to change every other day. Cells were cultured at 37 °C with 5% CO_2, and passaged every 4 ~ 5 days in PGM1 (Cat#CA1008500, CELLAPY, Beijing, China). Cells were tested for mycoplasma contamination (Cat#CA6101096, CELLAPY, Beijing, China) every month.

Alkaline phosphatase staining

Alkaline phosphatase staining was conducted following manufacturer's Instructions (Cat#C3206, Beyotime, Shanghai, China). In brief, hESCs were cultured in Matrigel-coated 24-well plates for 3 days. Cells medium was aspirated, and cells were washed three times with DPBS, followed by fixation with 4% paraformaldehyde (Cat#P0099, Beyotime, Shanghai, China) for 10 ~ 20 min. Then cells were washed with DPBS for 2 times. Add BCIP/NBT staining mix into the 24-well plate for 25 min at room temperature away from light. Later aspirating the staining solution, washing twice with DPBS. The staining results were observed and photographed under the microscope. Undifferentiated cells will be exhibited blue-purple, while differentiated cells will remain unstained.

hESC-derived cardiomyocytes differentiation

The hESCs were derived into cardiomyocytes according to the previously described protocol [36, 37], showing consistent efficiency across various hESC lines without the need for parameter optimization. Briefly, on day 0, the cell confluence reached 80–90%, and the cells were dissociated using PGM1 and resuspended in mTeSR™ Plus medium. Precise cell counting was crucial for ensuring stable differentiation efficiency. $2.5 \times 10^4/cm^2$ hESCs were seeded in Matrigel-coated 24-well plates and cultured for 2 days. At day 2, medium was changed into mTeSR™ Plus with 12 μmol/L CHIR99021 (Cat#S2924, Selleck, Shanghai, China) for 3 days. At day 5, cells were treated with RPMI 1640 (Cat#11875093, Gibco, Carlsbad, CA, USA)/B27 minus insulin (Cat#A18956-01, Gibco, Carlsbad, CA, USA) combined with 12 μmol/L CHIR99021 for 1 day. Next, the medium was changed into RPMI 1640/B27 minus insulin supplemented with 10 μmol/L XAV939 (Cat#S1180, Selleck, Shanghai, China) plus 10 μmol/L KY02111 (Cat#S7096, Selleck, Shanghai, China) for 4 days without medium changed. At day 10, cells were cultured in RPMI 1640/B27 minus insulin for 2 days. Then, medium was changed into RPMI 1640/B27(Cat# 17504044, Gibco, Carlsbad, CA, USA) and change the medium every 3 days, the beating cardiomyocytes would be observed around day 9 ~ 12 under microscope. Cells were cultured at 37 °C with 5% CO2 until used in related experiments. Different time points were defined: day 0 (hESC), day 5 (mesoderm, MES), day 10 (cardiac precursor, CP), day 14 (cardiomyocyte, CM).

Embryoid body (EB) culture

Embryoid body (EB) was applied to mimic three-layer differentiation, as previous hanging drop assay was used [38]. Preparing sufficient number of hESCs for digesting into single cells with PGM1, mTeSR™ Plus medium resuspended cells at a density of 100 cells/μl with 10 μM Y-27,632 (Cat# HY-10071, MCE, State of New Jersey, USA). Droplets (20 μl per droplet) were formed on 10 cm dish and cultured at 37 °C in 5% CO2 for 1 ~ 2 days. Next, EBs were transferred into Matrigel-coated plates, 20 ~ 30 droplets per well, and the medium was needed to be changed every three days (medium: DMEM, 10%FBS, 1% penicillin-streptomycin). About day 9, all the droplets were collected to carry out qRT-PCR for detection of ectodermal, mesodermal, and endodermal marker genes expression.

Mouse embryonic stem cell culture

Mouse D3 embryonic stem cells (ESCs) were cultured on feeder cells in dishes pre-coated with 0.1% gelatin (Cat#924504, Sigma-Aldrich, USA) within the media (500 ml of DMEM-high-glucose medium [Cat#11965118, Thermo Fisher Scientific, MA, USA], 94 mL of fetal bovine serum [Cat#10099141 C, Gibco, Carlsbad, CA, USA], 12.5 mL of penicillin/streptomycin [Cat#15070063, Gibco, Carlsbad, CA, USA], 6.25 mL of L-glutamine [Cat#25030081, Gibco, Carlsbad, CA, USA], 6.25 mL of non-essential amino acids [Cat#11140050, Gibco, Carlsbad, CA, USA], 62.5 μL of leukemia inhibitory factor [Cat# L5158, Sigma-Aldrich, USA], and 4.4 μL of b-mercaptoethanol [Cat#M6250, Sigma-Aldrich, USA]) [39] and medium was needed to change every other day. Cells were cultured at 37 °C with 5% CO_2, and passaged every 2 ~ 3 days using 0.25% trypsin-EDTA (Cat#T4049, Sigma-Aldrich, USA). The feeder cells were prepared following established protocols [40].

mESC-derived cardiomyocytes differentiation

The mESCs were differentiated into cardiomyocytes using the "hanging drop" method [39] and aggregated into embryoid bodies (EBs). Initially, mESCs were dissociated with 0.25% trypsin-EDTA and subsequently resuspended in differentiation medium, prepared as previously described [39]. The cells were cultured as hanging drops to form embryoid bodies (EBs) for 48 h. Following EB formation, the aggregates were harvested and plated onto six-well plates coated with 0.1% gelatin (15 EBs per well). Different time points were defined: day 0 (mESC), days 4–6 (mesoderm, MES), days 8–10 (cardiac precursor, CP), days 12–15 (cardiomyocyte, CM).

Plasmid constructs and transduction

For knockdown of SAMD4A, we utilized the tool website https://www.sigmaaldrich.cn/ to select 3 shRNA sequences, the target sequences were: seq1: 5'-GCTC ATAGACAAGTGTCTAAT-3'; seq2: 5'- GTGGAGGG TATTAGAGGAAAT –3'; seq3: 5'- CAGTGGTGTTC TACAATATTA –3'. Knockdown of FGF2, seq: 5'- TA ACTGGGCTTTCTCTAATTT-3'. The pLKO.1-puro-CMV-EGFP plasmid was transfected into hESCs using the Lipofectamine™ Stem Transfection Reagent (Cat#

STEM00001, Invitrogen, Carlsbad, California, USA) for 48 h, following the manufacturer's protocol. In order to overexpress SAMD4A, human SAMD4A (NM_015589) was amplified by PCR from human cDNA and cloned into Ubi-MCS-SV40-EGFP-IRES-puromycin. Approximately 1 μg plasmid was transfected to hESCs. Knockdown and overexpression efficiency was then detected using qRT-PCR and western blot. DNA sequencing was used to verify all constructs. Further details on plasmid construction can be provided upon request. All of the primer sets are listed in the Table S1.

SAMD4A knockdown/overexpression hESC lines

For the generation of knockdown/overexpression SAMD4A hESC lines, we chose lentiviral infection to transduce the hESCs. Firstly, HEK293T cells (ATCC) were plated in 10 cm dish and co-transfected with 3 plasmids, lentiviral SAMD4A KD/OE and lentiviral packaging plasmids psPAX2 (Cat #12260, Addgene), pMD2.G (Cat #12259, Addgene) using Lipofectamine 2000 (Cat#11668030, Thermo Fisher Scientific, MA, USA) according to the manufacturer's protocol. The transfected HEK293T cells were cultured for 2 days, with medium collected each day. Collected medium was centrifuged at 4000 g for 30 min to eliminate cells and cell debris. Supernatant containing virus was concentrated using PEG-8000 according to the manufacturer's protocol (Cat#25322-68-3, Yeasen, Shanghai, China). hESCs were seeded onto 6-well plates and infected with lentivirus carrying either shRNA targeting SAMD4A or an SAMD4A overexpression plasmid. After infected 24 h, observe the percentage of GFP under fluorescence microscope. After 48 h, 2 μg/ml puromycin was added for drug screening for 1 ~ 2 weeks, and the GFP-positive clones were picked for expansion culture, and the cells were gathered for further experiments.

RNA extraction and real-time PCR (qPCR)

Total RNA was isolated using Trizol reagent (Cat#9108, Takara, Shiga, Japan) following to manufacturer's instructions. RNA was reverse transcribed into cDNA using PrimeScript™ RT reagent Kit with gDNA Eraser (Cat#RR047A, Takara, Shiga, Japan). Quantitative RT-PCR was performed with ChamQ Universal SYBR qPCR Master Mix (Cat# Q321-02, Vazyme Biotech, Nanjing, China) on a CFX96 (Bio-Rad, California, USA) real-time PCR system. Relative mRNA levels were normalized to GAPDH. Primer sequences utilized were detailed in the Table S1.

Western blot

Cells were harvested for protein extraction with RIPA lysis buffer (Cat#P0013D, Beyotime, Shanghai, China) containing protease (Cat# P1005, Beyotime, Shanghai, China) and phosphatase inhibitor cocktail (Cat# P1045, Beyotime, Shanghai, China) on the ice. Then the mix was centrifuged at 4 °C at 12,000 g for 10 min and supernatant concentration was measured via BCA protein assay kit (Cat# P0012S, Beyotime, Shanghai, China). Equal proteins were loaded into 7.5% SDS-PAGE gels, and transferred to PVDF membranes (Millipore, CA, USA). Next the membranes were incubated in 5% BSA for 1 ~ 2 h, followed by overnight incubation with primary antibodies overnight at 4 °C. Then, washed the membrane with TBST for 10 min, 3 times, and subsequently incubated with corresponding secondary antibodies for 1 h at room temperature. After washed the bands with TBST for 3 times and visualized the blot with SuperSignal™ West Pico PLUS ECL substrate (Cat#34580, Thermo Fisher Scientific, MA, USA). Images were detected by Amersham Imager600 (GE Life Sciences). The antibodies used were as follows: anti-GAPDH (1:20000, Cat#60004-I-Ig, Proteintech, Rosemont, IL, USA), anti-OCT4 (1:1000, Cat# ab27985 Abcam, Cambridge, UK), anti-SOX2 (1:1000, Cat# 11064-1-AP, Proteintech), Anti-Cardiac Troponin T (1:1000, Cat# ab10214, Abcam), anti- MYH6 (1:2000, Cat# 22281-1-AP, Proteintech), anti-AKT1 + AKT2 + AKT3 (1:10000, Cat# ab179463, Abcam), anti-AKT1 (phospho S473) (1:10000, Cat# ab81283, Abcam), anti- SAMD4A (1:1000, Cat# 17387-1-AP, Proteintech), anti- mTOR (1:1000, Cat# 2983 S, Cell Signaling Technology, Danvers, Massachusetts, USA), anti-Phospho-mTOR (Ser2448) (D9C2) (1:1000, Cat# 5536, Cell Signaling Technology), Donkey Anti-Goat IgG(H + L) (1:10000, Cat# SA00001-3, Proteintech), Goat Anti-Rabbit IgG(H + L) (1:10000, Cat# SA00001-2, Proteintech), Goat Anti-Mouse IgG(H + L) (1:1000, Cat# SA00001-1, Proteintech). Antibodies utilized were listed in the Table S1.

Flow cytometry assay

Beating cardiomyocytes at least day20 were dispersed into single cell with TrypLE Express (Cat# 12604021, Gibco, Carlsbad, CA, USA). Next, washed the cells with DPBS for 3 times and fixed with 4% polyformaldehyde fixing solution at least 30 min. Then permeabilized by Immunostaining Permeabilization Solution with Triton X-100 (Cat# P0096, Beyotime, Shanghai, China) for 10 min. And then washed the cells 3 times with PBST, stained with PE Mouse Anti-Cardiac Troponin T or isotype control (Cat# 564767, BD Biosciences, San Jose, CA, USA) for 30 min away from light at room temperature. After washed for 3 times, resuspended with DPBS and detected by CytoFLEX LX Flow Cytometer (Beckman, Brea, CA, USA). The hESCs were staining for the cell surface marker, the stage-specific embryonic antigen (SSEA)- 4 (Cat# MAB4304, Sigma-Aldrich, USA), secondary antibody was used: Goat Anti-Mouse IgG H&L (Alexa Fluor® 647) (Cat# ab150115, Abcam, Cambridge, UK).

Immunofluorescence

Cells were first washed with DPBS for 3 times, and then fixed with 4% PFA at least 30 min. Permeabilized by Immunostaining Permeabilization Solution with Triton X-100 and block with 1% BSA. Primary antibodies incubated at 4 °C away from light overnight and corresponding secondary antibodies incubated for 1 ~ 2 h in the dark next day. After washed for 3 times, the cells were counterstained with DAPI (Cat# C1002, Beyotime, Shanghai, China) for 10 min. Images were obtained with Leica TCS-SP8 SR (Leica Microsystems, Wetzlar, Germany) and analyzed with ImageJ software.

RNA immunoprecipitation

For RNA immunoprecipitation, Magna RIP RNA-Binding Protein Immunoprecipitation Kit (Cat#17–701, Millipore) was used followed by the manufacturer's instruction. hESCs were collected with PGMI in 10 cm dishes, washed the cells with pre-cooled DPBS, the cell number was at least 2×10^7. Then, lysed the hESCs with RIP lysis buffer, which contained RNase inhibitor and protease inhibitor cocktail on the ice for 5 min. Next, prepared magnetic beads for immunoprecipitation, using Normal Rabbit IgG as negative control and anti-SAMD4A to incubate the beads protein A/G. Thawed the frozen RIP lysate quickly and centrifuged at 14,000 rpm for 10 min at 4 °C, divided supernatant into 3 parts, 10 µl was stored at -80 °C as input, another two equal parts (100 µl) were incubated with prepared beads-antibody overnight at 4 °C. Next day, centrifuged complex briefly and discarded the supernatant, washed the beads at least six times with RIP wash buffer. Used proteinase K buffer to digest the protein at 55 °C for 30 min, and centrifuged briefly to transfer the supernatant. Added 400 µl of phenol: chloroform: isoamyl alcohol (125:24:25) to supernatant, and purified RNA following the manufacturer's instructions. The immunoprecipitated RNA was further analyzed by qPCR.

RNA-seq and data analysis

Total RNA was individually extracted using Trizol reagent. Subsequently, the RNA quality was assessed using an Agilent 2200 system and stored at -80 °C. RNA samples with an RIN (RNA integrity number) > 7.0 were deemed suitable for cDNA library preparation. The construction of cDNA libraries for each RNA sample was performed using the TruSeq Stranded mRNA Library Prep Kit (Illumina, Inc.) following the manufacturer's guidelines. The first-strand cDNA, purified thereafter, was amplified via PCR to generate the cDNA libraries. Subsequently, the libraries underwent quality assessment using the Agilent 2200 system and were sequenced via NovaSeq 6000 in a 150 bp paired-end run. Prior to read mapping, adaptor sequences and low-quality reads were eliminated from the raw reads to obtain clean reads. The clean reads were then used the Hisat2 aligning to human genome (GRCh38, Ensembl104) [41]. Gene counts was obtained by using HTseq [42] and to determine the gene expression in using RPKM method. DESeq2 algorithm was applied to calculated the differentially expressed genes (DEGs). Following the significant analysis, adjust p value < 0.05 and abs|log2(fold-change)| > 0.58 [43, 44]. In order to further obtain the DEGs with high confidence, the differentially expressed result matrix obtained after DESeq2 analysis was input as SIGNAL (https://signal.niaid.nih.gov) with the parameters set as "Cutoff Type"="FDR" FDR, false discovery rate, "High Confidence Cutoff Value"="0.01", "FDR", "High Confidence Cutoff Value" = "0.01", " Medium Confidence Cutoff Value"="0.05", "Column to Use for Secondary Criteria"= "absLog2FC > = 0.585"; finally obtaining SIGNAL hits. Gene ontology (GO) analysis was conducted to facilitate understanding the biological implications of the differentially expressed genes [45]. Pathway analysis was conducted using the KEGG database to identify the significant pathway associated with the differentially expressed genes [46]. The DEGs are listed in Table S2.

snRNA-seq analysis

The dataset was obtained from the Gene Expression Omnibus (GEO) database under accession number GSE203274 [27]. This comprehensive dataset encompasses two distinct cyanotic CHD subtypes - Hypoplastic left heart syndrome (HLHS) and Tetralogy of Fallot (TOF), along with two forms of cardiomyopathy: Dilated Cardiomyopathy (DCM) and Hypertrophic Cardiomyopathy (HCM). snRNA-seq data processing was performed using Seurat (v4.3.0). Initial quality control included filtering nuclei with fewer than 100 detected genes and excluding those exceeding 2% read content, resulting in 157,273 high-quality nuclei retained for downstream analysis. Variable feature selection identified the top 2,000 highly variable genes for subsequent principal component analysis (PCA, 20 principal components). To address potential batch effects, we implemented Harmony integration (v1.0) [47] using all 20 principal components. Dimensionality reduction was achieved through Uniform Manifold Approximation and Projection (UMAP) with default parameters, followed by graph-based clustering at a resolution of 0.2 (20 dimensions). Cell type identification was performed through an iterative process: differential expression analysis using the FindAllMarkers function (min.pct = 0.25, thresh. use = 0.10) [48].

Myocardial subpopulation analysis at a resolution of 0.05 identified three distinct cardiomyocyte subpopulations. Cellular proportions were visualized with stacked bar plots, and SAMD4A expression was assessed using

DotPlot and FeaturePlot to evaluate detection frequency and spatial distribution in UMAP embeddings.

Dual luciferase reporter assay

As for the binding sites, which were carried into pDuo vector. All the constructed plasmids were confirmed by DNA sequencing. Primers are listed in the Table S1. For the dual luciferase reporter assay, the constructed plasmids were co-transfected with SAMD4A knockdown or overexpression plasmid into the HEK293T cells cultured in the 24-well plates using PEI transfection reagent, and the pDuo -Fluc-TK-Rluc was used as control. After 24 ~ 36 h transfected, the cells were collected to detect the relative luciferase activity measured by the Dual Luciferase Reporter Gene Assay Kit (Cat#RG029S, Beyotime, Shanghai, China), and detected by Spark® Multimode Microplate Reader (TECAN Spark, Switzerland). All the experiments were performed independently three times.

Cell cycle analysis

For the cell cycle analysis, cells were performed using Cell Cycle and Apoptosis Analysis Kit (Cat# C1052, Beyotime, Shanghai, China) following the manufacturer's instructions. Briefly, digested 10^7 cells with Trypsin (without EDTA) for 2 min and discarded the medium. Digested into single cells and centrifuged at 1000 rpm for 10 min at 4 °C. Discarded supernatant and resuspended in pre-cooled PBS, filtered through 40 μm pore size cell strainer. Then, fixed the cells to pre-cooled 70% anhydrous ethanol overnight at 4℃. On the following day, centrifuged the cells to remove ethanol, washed once with PBS, and added 0.5 ml the complex of RNase-A in PBS (containing 0.1% Triton X-100) and PI, digested for 30 min at 37℃ away from light. Last, flow cytometry detection was performed by CytoFLEX LX Flow Cytometer (Beckman) and Flow Jo (v10) was used to analyze the cell cycle, GraphPad Prism 9 software was used to draw graphs.

RNA stability analysis

As for RNA stability analysis, 10^7 cells were seeded in 24-well plates until the cell density came to about 90%, changed medium containing 1 μmol/L Actinomycin D (Cat#HY-17559, MCE, State of New Jersey, USA) to inhibit transcription. RNA was collected at half-hourly intervals using Trizol. qRT-PCR was conducted to detect the target gene mRNA level which was normalized to GAPDH.

Contraction analysis

The contractile activity of H7-derived cardiomyocytes (H7-CMs) was assessed using IonOptix LLC's contractility/photometry system (IonOptix, Milton, MA) [49]. Briefly, H7-CMs were plated onto Matrigel-coated 15-mm confocal dishes. The cells were then analyzed under the IonOptix system at 37 °C with 5% CO_2. A single cardiomyocyte exhibiting spontaneous contractions was picked for measurement. Contractile activity was quantified by monitoring changes in pixel intensity at the cell periphery using the 'Cytomotion pixel intensity' mode, and the contraction amplitude was determined through pixel correlation analysis.

Statistical analysis

All the experiments were independently repeated at least three times. All the data were presented in mean ± SEM. All the statistical analyses were carried out by GraphPad Prism 9.0 software (San Diego, CA). Two groups comparison was used two-tailed Student's *t*-test. For more than two groups comparison was used one-way ANOVA test and two- way ANOVA test. The value of $P < 0.05$ was considered statistically significant.

Results

The expression of SAMD4A is gradually increased during cardiomyogenesis

To detect the molecular role of SAMD4A in cardiomyogenesis, we applied a cardiomyogenic model based on the specific differentiation of hESCs into cardiomyocytes (Fig. 1a and Supplementary Fig. S1a). Initially, the undifferentiated hESCs at day 0 exhibited high level of pluripotency marker genes *NANOG*, *SOX2*, and *OCT4*. Subsequent upregulation of *MESP1* by day 5 indicated a transition towards a mesodermal (MES) phenotype. By day 10, there was a significant increase in expression of cardiac progenitor (CP) markers *NKX2-5*, *TBX5*, and *ISL1*. Consequently, the functional cardiomyocyte-specific marker *TNNT2*, *MYH6*, and *MYH7*, exhibited an upregulation pattern at day 14, alongside the emergence of spontaneous beating in cardiomyocytes (Fig. 1b and Supplementary Fig. S1b). The proportion of cTNT-positive cardiomyocytes notably increased to 83.9% (Supplementary Fig. S1c). Importantly, the expression of SAMD4A is high during the periods of embryonic stem cells and cardiomyocytes (Fig. 1c). Additionally, we investigated the expression profile of SAMD4A across different organs throughout human embryonic development, ranging from post-conception 4 weeks (4 pcw) to toddlerhood, utilizing public available data. Remarkably, SAMD4A consistently exhibited elevated expression levels in the human heart (Supplementary Fig. S1d). We also employed the hanging drop method to induce the differentiation of mESCs into cardiomyocytes (Supplementary Fig. S2a, b). The expression of Samd4a was markedly upregulated during both the embryonic stem cell and cardiomyocyte stages (Supplementary Fig. S2c), a pattern that aligned with observations in humans. Furthermore, we analyzed the expression pattern of Samd4a across multiple organs during mouse embryonic development, ranging from embryonic day 10.5 (E10.5) to postnatal day 14 (P14), using publicly available datasets. Notably,

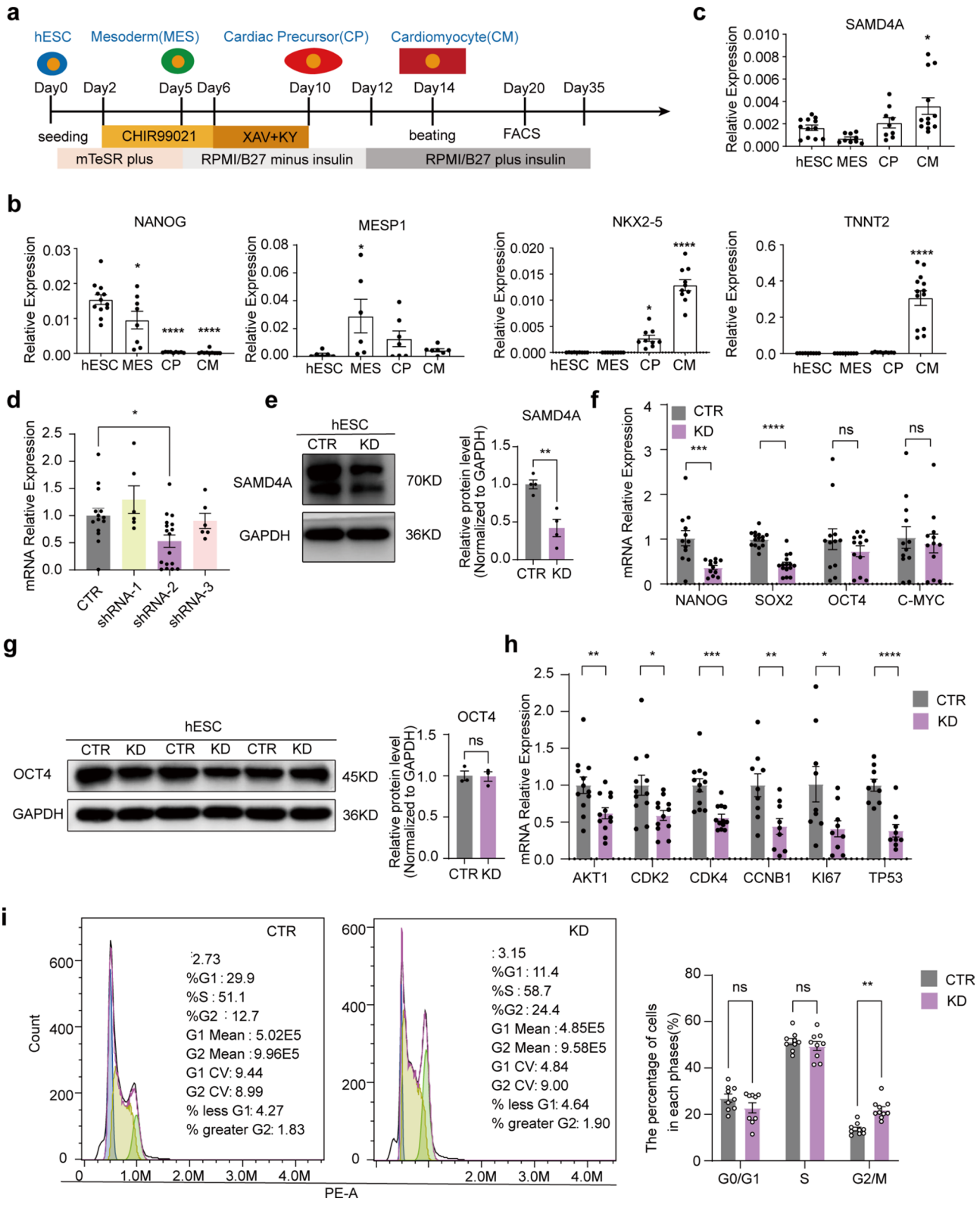

Fig. 1 (See legend on next page.)

(See figure on previous page.)

Fig. 1 The impact of SAMD4A knockdown on hESCs and cellular characteristics. **(a)** A schematic representation of the monolayer culture method used for generating hESC-derived cardiomyocytes. **(b)** Key marker genes, including *NANOG* (pluripotency), *MESP1* (mesoderm), *NKX2-5* (cardiac progenitor), and *TNNT2* (cardiomyocytes), were assessed using qRT-PCR analysis at different time points during cardiomyocyte generation. **(c)** and **(d)** Focus on qRT-PCR analysis of SAMD4A mRNA expression during hESC-derived cardiomyocytes generation and the knockdown efficiency achieved by three *SAMD4A* short hairpin RNAs (shRNAs). **(e)** Left, the relative protein levels of SAMD4A in *SAMD4A*-KD-hESCs and control hESCs are compared. Right, a relative signal intensity analysis of SAMD4A protein levels with GAPDH as a control. Corresponding uncropped full-length gels and blots are presented in Supplementary Fig. S9. **(f)** qRT-PCR was utilized to investigate the impact of *SAMD4A* KD on pluripotency markers (*NANOG*, *SOX2*, *OCT4*, *C-MYC*) at the mRNA level. **(g)** Left, the relative protein level of OCT4 in *SAMD4A*-KD-hESCs and control hESCs. Right, relative signal intensity analysis of OCT4 protein levels with GAPDH as a control. Corresponding uncropped full-length gels and blots are presented in Supplementary Fig. S9. **(h)** qRT-PCR was employed to assess the mRNA expression of proliferation markers (*AKT1*, *CDK2*, *CDK4*, *CCNB1*, *KI67*, *TP53*) in *SAMD4A*-KD-hESCs and *SAMD4A*-CTR-hESCs. **(i)** Propidium iodide staining to determine cell cycle phases in control and *SAMD4A*-KD-hESCs. The distribution of cells in the G0/G1, S, and G2/M phases was calculated using FlowJo (v10). **(b)** and **(c)** Statistical significance was determined by the ordinary one-way ANOVA test. **(d)**- **(i)** Statistical significance was analysed by the two-tailed Student's *t*-test, indicating significant differences with $*P < 0.05$, $**P < 0.01$, $***P < 0.001$, and $****P < 0.0001$ vs. control group (mean ± SEM;$n = 3$ from at least three independent experiments)

Samd4a exhibited consistently high expression levels in the mouse heart (Supplementary Fig. S2d).

We further investigated whether the expression of SAMD4A has potential pathological relevance in CHD. We analyzed snRNA-seq data from a total of 157,273 nuclei isolated from both healthy control hearts and hearts of patients with CHD. Unbiased graph-based iterative clustering was applied to cardiomyocytes from the complete snRNA-seq dataset of cardiac tissue, revealing three distinct cardiomyocyte clusters (CM1, CM2, and CM3) (Supplementary Fig. S3a). The CM1 cluster, representing the most stressed cardiomyocyte population, was exclusively composed of cardiomyocytes from CHD patients, with significant enrichment in cases of TOF, DCM, HCM, and HLHS. Remarkably, cardiomyocytes from TOF and DCM were predominantly classified into CM1, supporting the conclusion that the CM1 cell state is primarily driven by CHD pathology. In contrast, the CM2 cluster was enriched with cardiomyocytes from control hearts. The CM3 cluster included cardiomyocytes from both control hearts and all CHD categories (Supplementary Fig. S3b). In addition, SAMD4A expression was significantly decreased in CM1 and CM3, clusters enriched in CHD, compared to CM2 (Supplementary Fig. S3c), highlighting the downregulation of SAMD4A in CHD. Furthermore, we utilized a published single-cell sequencing dataset from human hearts [50], which quantified the expression levels of 3,004 identified RBPs in endothelial cells, inflammatory cells, fibroblasts, and cardiomyocytes [26]. Through data integration, a heatmap was constructed to illustrating the expression levels of SAMD4A and pivotal RBPs associated with cardiac development in human cardiac cells, revealing high expression of SAMD4A in ventricular cardiomyocytes (Supplementary Fig. S3d). These observations suggest SAMD4A may play an important role in the early stages of heart development and support its relevance in the pathogenesis of CHD.

SAMD4A is not essential for pluripotency States but influences hESC proliferation

Initially, three shRNAs were designed to down-regulate SAMD4A expression in hESC. Subsequently, an H7 hESC stable-transfer cell line was established using puromycin screening for a 2-week period. The efficiency of SAMD4A knockdown was assessed through real-time quantitative Polymerase Chain Reaction (qRT-PCR) and Western blot methods (Fig. 1d, e). The morphology of hESCs with SAMDA4A knockdown (*SAMD4A*-KD-hESCs) appeared normal, as evidenced by positive alkaline phosphatase staining, which showed no significant difference compared to the control (Supplementary Fig. S1e). Additionally, the cell surface marker of hESCs, the stage-specific embryonic antigen-4 (SSEA4), demonstrated no significant variation in $SSEA4^+$ population between *SAMD4A*-KD-hESCs and the control group (Supplementary Fig. S1f). Both qRT-PCR and Western blot analyses showed that SAMD4A knockdown in hESCs had no discernible effect on the expression of pluripotency marker genes *OCT4*. Additionally, no significant changes were observed in the mRNA expression of *C-MYC*, while the mRNA expression of *NANOG* and *SOX2* was reduced (Fig. 1f, g). Furthermore, *SAMD4A*-KD affected cell cycle dynamics and proliferative capacity of the hESCs, which were verified with a significant expression decrease for the proliferative-related genes *AKT1*, *CDK2*, *CDK4*, *CCNB1*, *KI67*, and *TP53* (Fig. 1h), along with an augmented population of cells in the G2/M phase, indicating that the cells were substantially arrested at the G2/M phase, compromising hESC proliferation (Fig. 1i). Collectively, these results demonstrate SAMD4A plays a dispensable role in maintaining the pluripotency of hESCs, but the knockdown of SAMD4A inhibits proliferation.

SAMD4A knockdown affects the stem cell fate decision and impairs cardiomyocyte differentiation

To investigate the function of SAMD4A in stem cell fate determination, *SAMD4A*-KD-hESCs were subjected to random differentiation into three germ layers (ectoderm, mesoderm, and endoderm) using the hanging drop method [38] (Fig. 2a). qRT-PCR analysis of EBs on day11 did not influence the expression of pluripotency markers *NANOG*, *SOX2*, *OCT4*, *C-MYC*, *KLF4* (Supplementary Fig. S4a). The mRNA expression analysis revealed

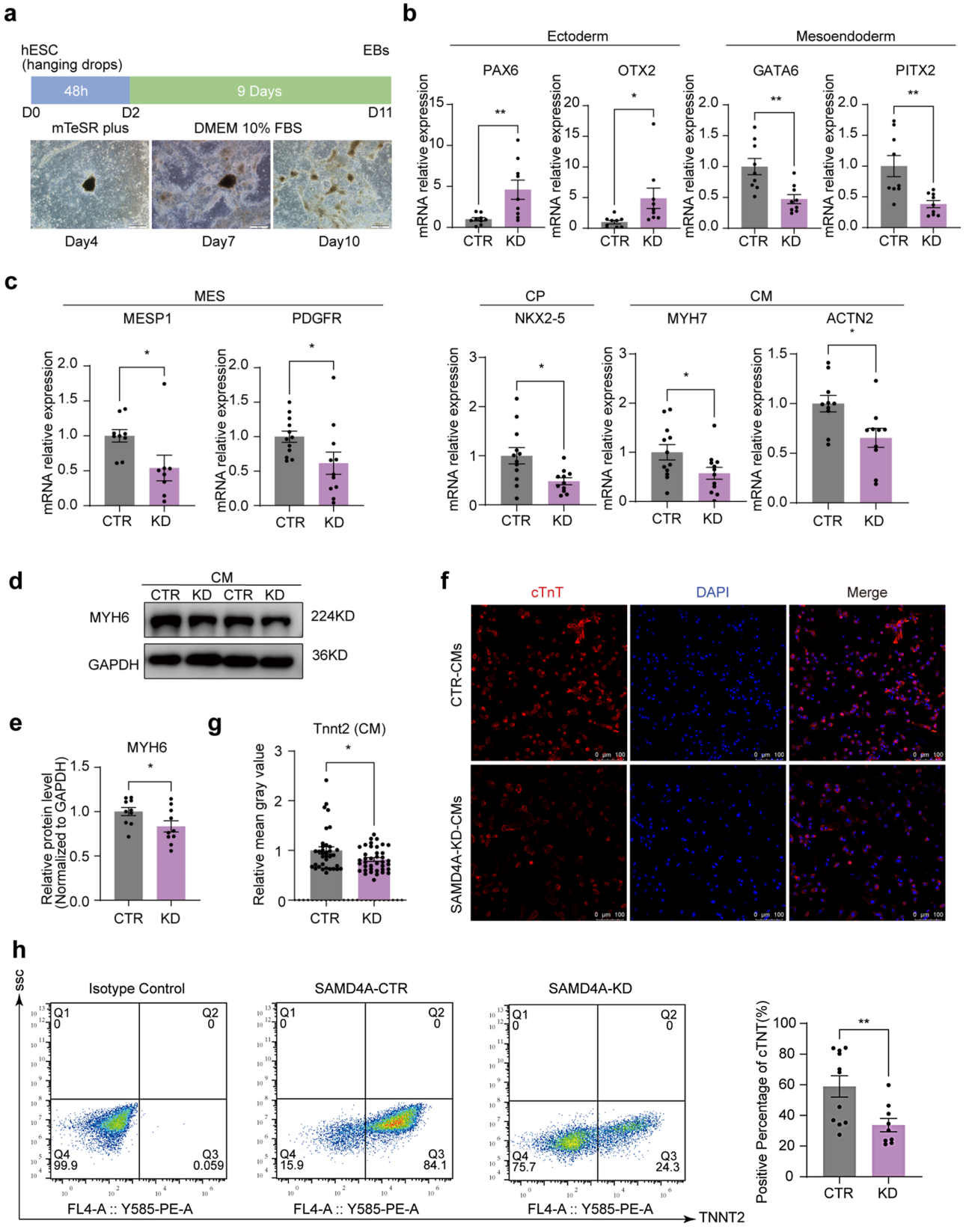

Fig. 2 (See legend on next page.)

(See figure on previous page.)

Fig. 2 SAMD4A is required for the normal differentiation of hESCs. **(a)** Schematic illustration outlines differentiation of hESCs using the EB model. **(b)** qRT-PCR mRNA analysis of ectodermal (*PAX6*, *OTX2*) and mesoendoderm (*GATA6*, *PITX2*) marker gene expression in *SAMD4A*-CTR-EBs and *SAMD4A*-KD-EBs on day11. **(c)** qRT-PCR analysis of mesoderm-specific genes (*MESP1*, *PDGFR*), cardiac progenitor genes (NK*X2-5*), and cardiomyocyte-specific genes (*MYH7*, *ACTN2*) at different time points during cardiomyogenesis in control and *SAMD4A*-KD-hESCs. **(d)** Western blot analysis of the cardiomyocyte-specific marker MYH6 was performed in control and *SAMD4A*-KD-hESCs-derived cardiomyocytes. Corresponding uncropped full-length gels and blots are presented in Supplementary Fig. S9. **(e)** Relative signal intensity analysis of MYH6 protein levels with GAPDH as a control. **(f)** Displays representative fluorescence images of cTnT (red) and DAPI (blue) immunostaining in control and *SAMD4A*-KD-hESCs-derived cardiomyocytes. Scale bars: 100 μm. **(g)** Relative fluorescence intensity analysis of cTnT in control and *SAMD4A*-KD-hESCs-derived cardiomyocytes is presented. Statistical analysis data were derived from a minimum of 9 fields in each of three independent cell culture experiments. **(h)** FACS analysis of hESC-derived cardiomyocytes, focusing on the specific cardiomyocyte marker cTnT in *SAMD4A*-CTR-hESCs and *SAMD4A*-KD-hESCs-derived cardiomyocytes. Left, the analysis of different populations in FlowJo (v10), with the isotype control as the negative control. Right, statistical analysis of the positive percentage of cTnT. Statistical significance was analysed by the two-tailed Student's *t*-test, indicating significant differences with $^{*}P<0.05$, $^{**}P<0.01$, $^{***}P<0.001$, and $^{****}P<0.0001$ vs. control group (mean ± SEM;$n=3$ from at least three independent experiments)

an up-regulation of ectodermal marker genes *PAX6* and *OTX2*, along with a down-regulation of mesoendodermal marker genes *GATA6* and *PITX2* in these cells (Fig. 2b). These findings indicate the pivotal role of SAMD4A in orchestrating mesoendoderm-lineage specification while inhibiting ectodermal differentiation, thus impacting stem cell lineage commitment.

Giving the increasing expression of SAMD4A during cardiomyocyte differentiation and specific high expression during human heart development, suggested that SAMD4A is necessary for mesodermal cardiomyocyte lineage specification. Next, a monolayer-culture cardiomyogenic model was applied to evaluate the expression of specific markers for MES, CP, and CM during the *SAMD4A*-KD-hESCs-CM differentiation (Supplementary Fig. S4b). *SAMD4A*-KD-hESCs have exhibited significant down-regulation of cardiac mesodermal marker genes *MESP1* and *PDGFR*, cardiac progenitor *NKX2-5*, and cardiomyocyte genes *MYH7*, *ACTN2*, and *MYH6* (Fig. 2c-e). In addition, *SAMD4A*-KD mesoderm cells exhibited a notable decrease in the mRNA level of mesoendoderm markers (*FOXA2*, *SOX17*) (Supplementary Fig. 4c). Accordingly, the number of cTnT positive cells also markedly decreased (Fig. 2f, g), and the beating frequency slowed down significantly (Supplementary Fig. S4d, Supplementary Videos S1, S2). Flow cytometry analysis demonstrated a noticeably reduced efficiency of cardiomyocyte differentiation, with only 24.3% cTNT positive cells in absence of SAMD4A (Fig. 2h). Additionally, genes involved in cardiac myofibrillogenesis and cardiomyocyte contractile function, such as *NEBL*, *PDLIM5*, and *TNNI1*, as well as calcium regulatory genes including *RYR2*, *SERCA2*, *CASQ2*, and *CAMK2D*, were down-regulated in *SAMD4A*-KD-CMs, as confirmed by qPCR (Supplementary Fig. S4e). We also evaluated cardiomyocyte contractility and detected a notable decrease in contraction amplitude in *SAMD4A*-KD-CMs relative to the control group (Supplementary Fig. S4f, g).

Furthermore, we explored the impact of SAMD4A on cardiac lineage commitment beyond hESC stage. We transfected *SAMD4A* shRNA into mesodermal cells at mesoderm stage (Supplementary Fig. S5a, b, and c). Congruent with our previous findings, knockdown of *SAMD4A* on day5 resulted in the suppression of cardiac mesodermal marker genes *T*, *MESP1*, *NODAL*, *PDGFR*, and *EOMES*, cardiac transcription factors (TFs) *NKX2-5*, *ISL1*, and cardiac-specific genes *MYH6*, *MYH7*, *TNNT2*, and *ACTN2* (Supplementary Fig. S5d, e, and f). These data demonstrate SAMD4A is essential for cardiomyocyte lineage specification and myocardial function.

SAMD4A knockdown alters hESC transcriptome and expression pattern of specific functional genes

To understand SAMD4A's molecular function in cardiomyogenesis from hESCs, we conducted RNA-seq assays on *SAMD4A*-control-hESCs (*SAMD4A*-CTR-hESCs) and *SAMD4A*-KD-hESCs, aiming to identify potential mechanisms by which SAMD4A regulates cardiomyogenic processes in hESCs (Supplementary Fig. S4h). In the condition, 485 genes were up-regulated, while 615 genes were decreased (Fig. 3a; Supplementary Table S2). Among them, key stem cell lineage differentiation genes such as *WNT8A*, *DNMT3B*, and *FGF8* were identified to be increased, whereas meso-endoderm differentiation-specific genes, including *SETD7*, *FOXO3*, *RUNX2*, *FGF2*, and *GATA4* were induced to undergo down-regulation (Fig. 3a). The heatmap analysis for DEGs confirmed again the decrease of the cell cycle marker *CCND1*, as well as the upregulation of ectoderm markers *NES*, *GLI2*, and *TUBB3* (Fig. 3b).The Kyoto Encyclopedia of Genes and Genomes (KEGG) pathway analysis declared that the DEGs are associated with pathways such as MAPK signaling, Calcium signaling, PI3K-AKT signaling, and Rap1 signaling (Fig. 3c), which have been valeted to be associated with cardiomyocyte differentiation [51–54]. Additionally, the Gene Ontology (GO) enrichment analysis of the DEGs detected in these biological processes (BP) are related to mediate cell differentiation, heart development, and developmental processes (Fig. 3d). Consequently, SAMD4A is intricately involved in above related pathways to modulate cardiomyogenesis from hESCs.

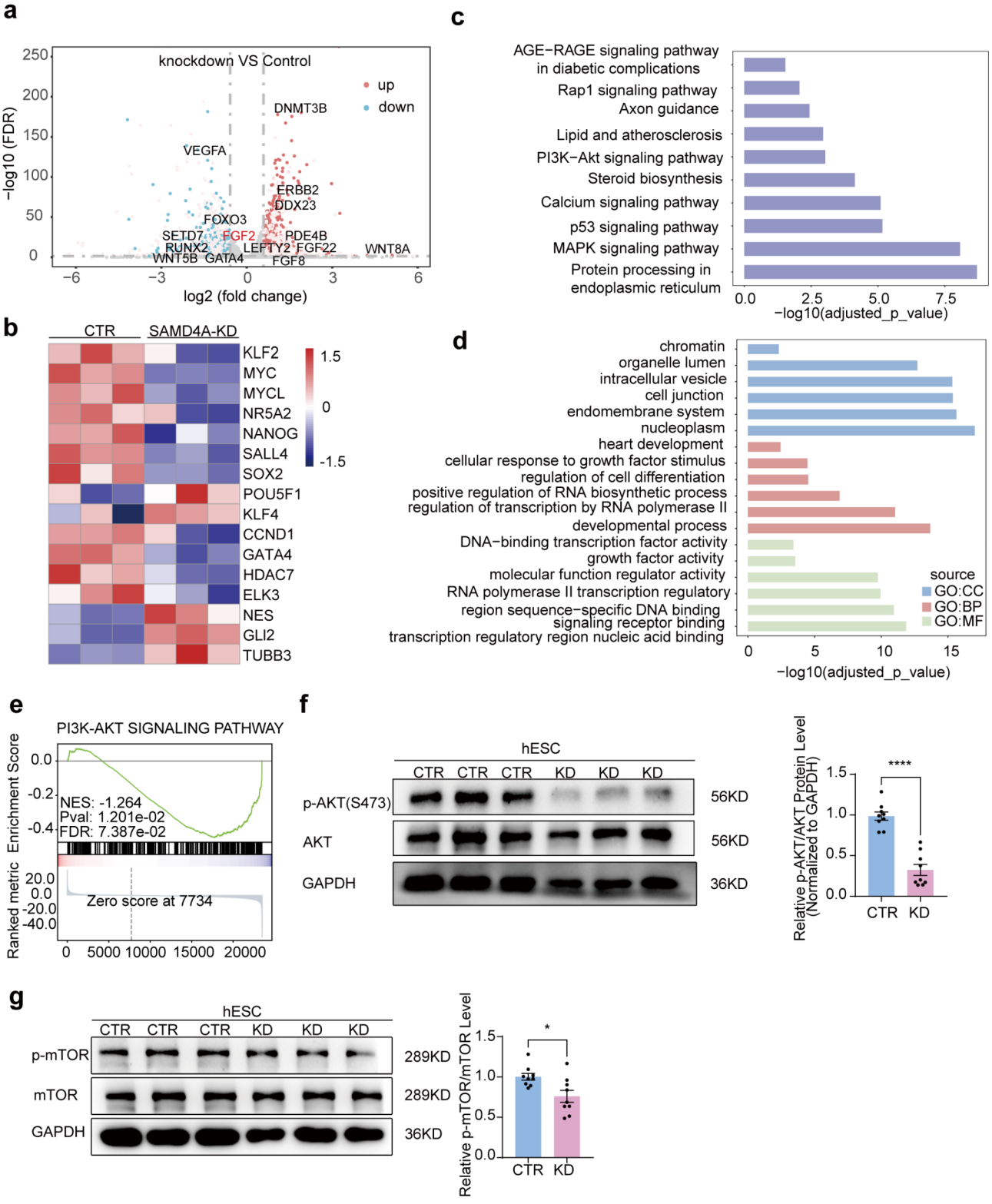

Fig. 3 (See legend on next page.)

(See figure on previous page.)

Fig. 3 Transcriptomic analysis reveals that the knockdown of SAMD4A represses the PI3K/AKT/mTOR signaling. **(a)** The Volcano plot illustrates differentially the DEGs between *SAMD4A*-KD-hESCs and *SAMD4A*-CTR- hESCs. Based on the FDR value (< 0.05) and abs|log2(fold-change)| > 0.58, 485 genes were up-regulated, and 615 genes were down-regulated in *SAMD4A*-KD-hESCs. **(b)** A representative heatmap displayed DEGs associated with pluripotency, proliferation, and ectoderm markers. **(c)** KEGG analysis was conducted on the DEGs in *SAMD4A*-KD-hESCs compared to the respective control hESCs, revealing the top 10 enriched pathways with corresponding P values. **(d)** GO enrichment analysis of the DEGs in *SAMD4A*-KD-hESCs compared with the respective control hESCs was presented for cellular component (CC), biological process (BP), and Molecular Function (MF). **(e)** Gene Set Enrichment Analysis (GSEA) revealed the involvement of genes in the PI3K/AKT signaling pathway in *SAMD4A*-KD-hESCs versus control hESCs, with the normalized enrichment score (NES) provided. **(f)** The left panel shown the relative protein level of AKT and the phosphorylation level of AKT (p-AKT) in *SAMD4A*-KD-hESCs compared with the respective control hESCs. Right, a quantitative analysis of the phosphorylation level of AKT. Corresponding uncropped full-length gels and blots are presented in Supplementary Fig. S9. **(g)** The left panel illustrated the relative protein level of mTOR and the phosphorylation level of mTOR (p-mTOR) in *SAMD4A*-KD-hESCs compared with the respective control hESCs, normalized to GAPDH. Right, a quantitative analysis of the phosphorylation level of mTOR. Corresponding uncropped full-length gels and blots are presented in Supplementary Fig. S9. Statistical significance was analysed by the two-tailed Student's *t*-test, indicating significant differences with $^{*}P < 0.05$, $^{**}P < 0.01$, $^{***}P < 0.001$, and $^{****}P < 0.0001$ vs. control group (mean ± SEM;$n = 3$ from at least three independent experiments)

SAMD4A regulates hESC cell fate through PI3K/AKT/mTOR signaling

Furthermore, Gene Set Enrichment Analysis (GSEA) of the DEG was used to scrutinize the impacted signaling pathways in *SAMD4A*-KD-hESCs, which revealed that the genes associated with the PI3K/AKT/mTOR signaling were significantly down-regulated, aligning with the findings from KEGG analysis (Fig. 3e). Notably, the PI3K/AKT/mTOR pathway exerts a crucial influence on maintaining stem cell pluripotency and proliferation. We really detected a significant inhibition on AKT and mTOR phosphorylation in *SAMD4A*-KD-hESCs (Fig. 3f, g), which is consistent with previous evidence involved in expression alteration in *Samd4a* mutant mice [29]. Collectively, SAMD4A potentially mediates PI3K/AKT/mTOR signaling axis to modulate the fate of hESCs towards cardiomyocytes.

SAMD4A functions by targeting *FGF2*

To further unravel the molecular details underlying SAMD4A-induced cardiomyocyte lineage differentiation, we applied the RNAact bioinformatic tool to identify potential targets of SAMD4A [55], and found that SAMD4A indeed targeted the mRNAs (targets were listed in Table S2) which involved in the pathways mediating stem cell differentiation, specifically cardiac developmental (Fig. 4a). Further analysis indicated that *FGF2* might be a potential target of SAMD4A (Fig. 4b). Intriguingly, FGF2 was recognized as a crucial factor in the PI3K/AKT/mTOR pathway and was down-regulated during cardiomyocyte differentiation (Fig. 4c). Then, we detected that the expression pattern of *FGF2* was positively associated with the knockdown or overexpression of SAMD4A in hESCs-derived cardiomyocytes (Fig. 4d, e), and SAMD4A really combined with *FGF2* by RNA immunoprecipitation (RIP) (Fig. 4f). In addition, other potential targets of RNA- binding protein SAMD4A were validated through RNA immunoprecipitation (RIP)-quantitative PCR (qPCR), the results showed that *FGF18*, *NANOG*, *OCT4*, *SMAD6* could bind with SAMD4A (Supplementary Fig. S6). FGF2 is a crucial factor that governs the processes of proliferation and cardiac lineage commitment differentiation in hESCs, activating mTOR through FRS2α-mediated PI3K/AKT signaling pathway [56–63]. Furthermore, we investigated whether SAMD4A functions directly via *FGF2*-dependent PI3K/AKT/mTOR signaling pathway, we implemented rescue experiments through supplementing 100ng/ml FGF2, the concentration maintaining in mTeSR [64], to *SAMD4A*-CTR-hESCs and *SAMD4A*-KD- hESCs and FGF inhibitor (25μM SU5402) in *SAMD4A*-CTR-hESCs and *SAMD4A*-OE-hESCs. Subsequently, we assessed the mRNA levels of proliferation marker genes, as illustrated in the Fig. 4g, the *KI67*, *CCNB1*, *CCND1* was significantly increased in *SAMD4A*-CTR-hESCs, and the defect in expression of proliferation markers resulted in the downregulation of SAMD4A was partly rescued following treatment with FGF2 in *SAMD4A*-KD-hESCs (Fig. 4h). We then detected the impact of FGF2 inhibitor on hESCs proliferation, SU5402 repressed the expression of *CDK1* and abolished the upregulation of proliferation markers *KI67*, *AKT1*, *CDK1*, *CDK4* in *SAMD4A*-OE-hESCs (Supplementary Fig. S7a). We further assessed whether the FGF2 inhibitor could rescue the influence of SAMD4A on PI3K/AKT/mTOR signaling. We added SU5402 to inhibit FGF2 in *SAMD4A*-OE-hESCs and detected that the inhibition of FGF2 suppressed the levels of AKT phosphorylation in *SAMD4A*-OE-hESCs (Supplementary Fig. S7b). In addition, we verified the influence of *FGF2* knockdown on *SAMD4A*-OE-hESCs. *FGF2*-shRNA was constructed, achieving knockdown efficiency of approximately 55% (Supplementary Fig. S7c). After *FGF2* knockdown in *SAMD4A*-OE-hESCs, the upregulation of proliferation markers *KI67*, *AKT1*, *CDK1*, *CDK2*, *CDK4*, and *CCNB1* was negated and the levels of AKT phosphorylation in *SAMD4A*-OE-hESCs were significantly reduced (Fig. 4i, j). These findings provide that *FGF2* acts downstream of SAMD4A, and the impact of SAMD4A on PI3K/AKT/mTOR signaling is achieved through *FGF2*.

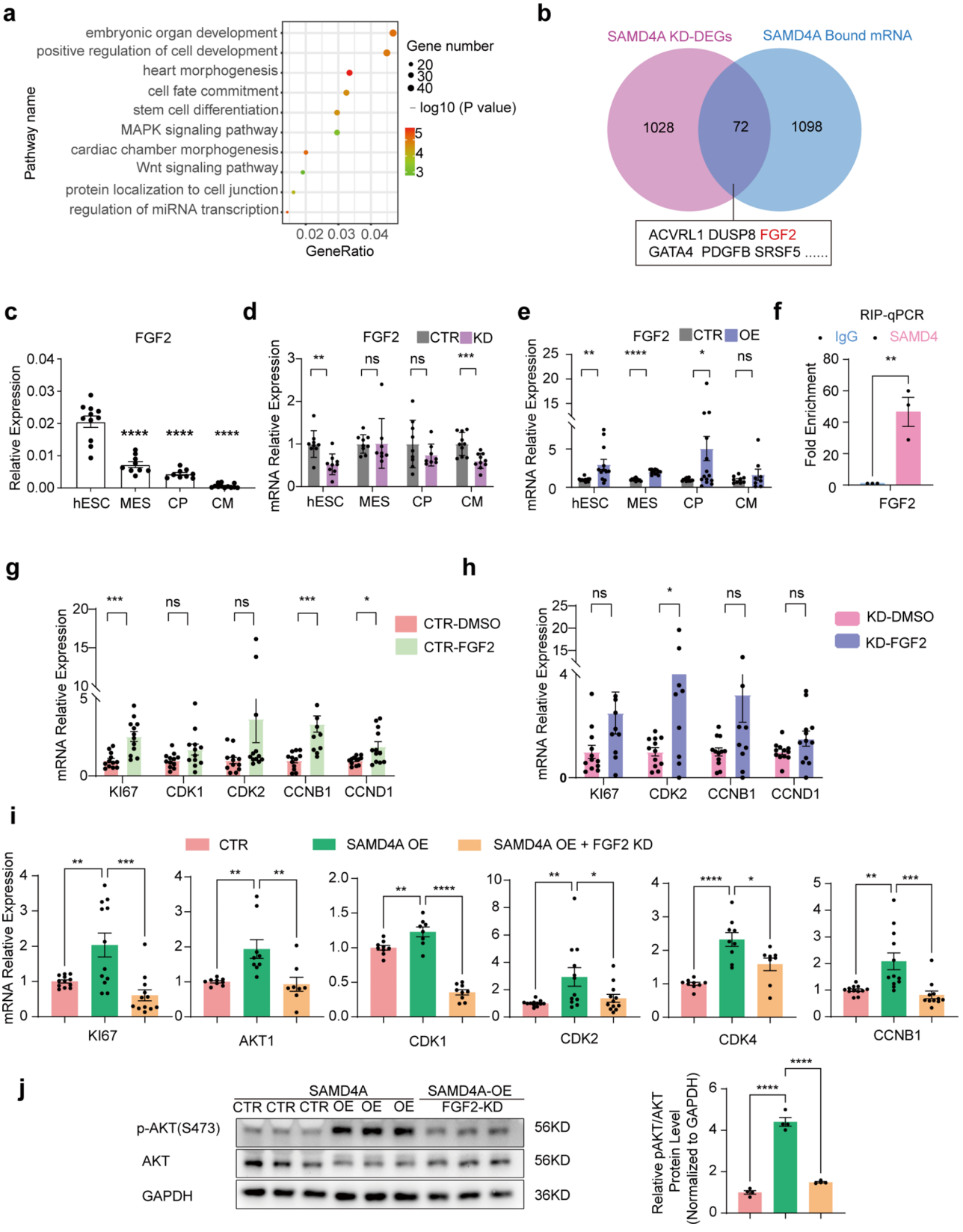

Fig. 4 (See legend on next page.)

(See figure on previous page.)

Fig. 4 Functions of SAMD4A by targeting *FGF2*. **(a)** Enrichment analysis of KEGG pathways was performed on mRNAs bound by SAMD4A. **(b)** Venn diagram illustrated the overlap between candidate targets of SAMD4A-bound mRNAs and DEGs in *SAMD4A*-KD-hESCs highlighting *FGF2* as a potential SAMD4A-bound target. **(c)** qRT-PCR revealed the mRNA expression of *FGF2* at different time points during cardiomyocyte differentiation in H7 ESC lines. Statistical analysis was conducted through the two-tailed Student's *t*-test. **(d)** qRT-PCR displayed the mRNA level of *FGF2* during cardiomyocyte differentiation in *SAMD4A*-KD-hESCs and the scramble control. **(e)** qRT-PCR demonstrated the mRNA level of *FGF2* during cardiomyocyte differentiation in *SAMD4A*-OE-hESCs and the scramble control. **(f)** RNA immunoprecipitation followed by qRT-PCR (RIP-qPCR) was conducted to confirm SAMD4A binding to the *FGF2* mRNA transcript. Target mRNAs with a > 1-fold change (calculated by $2^{-\Delta\Delta Ct}$) compared to the IgG control were acknowledged "confirmed targets," while no enrichment was tested as two non-target mRNAs showing a < 1-fold change. **(g)** and **(h)** qRT-PCR displayed the mRNA expression of proliferation marker genes *KI67*, *CDK1*, *CDK2*, *CCNB1*, and *CCND1*. *SAMD4A*-KD-hESCs and the scramble control hESCs were cultured in 100ng/ml FGF2 and DMSO. **(i)** qRT-PCR illustrated the mRNA expression of proliferation marker genes *KI67*, *AKT1*, *CDK1*, *CDK2*, *CDK4*, and *CCNB1*. *SAMD4A*-OE-hESCs were transfected with *FGF2* shRNA. **(j)** Western blot assay of the phosphorylation level of AKT (p-AKT) in control and *SAMD4A*-OE-hESCs (left panel). GAPDH was used as the respective control. *SAMD4A*-OE-hESCs were transfected with *FGF2* shRNA. Right, a quantitative analysis of the phosphorylation level of AKT. Corresponding uncropped full-length gels and blots are presented in Supplementary Fig. S9. **(c)-(h)** Statistical significance was determined by the two-tailed Student's *t*-test. **(i)** and **(j)** Statistical significance was determined by the one-way ANOVA. *$P < 0.05$, **$P < 0.01$, ***$P < 0.001$, and ****$P < 0.0001$ (mean ± SEM; $n = 3$ from at least three independent experiments)

SAMD4A regulates *FGF2* translation and mRNA stability

To elucidate how SAMD4A mediates *FGF2* to exert its impact on the PI3K/AKT/mTOR pathway, as an RBP, SAMD4A has been verified to have a potential capability to interact with target mRNAs, leading to modifications in post-transcriptional regulation of gene expression [32, 33, 65]. SAMD4A harbours a sequence preference for binding to targets, particularly recognizing a 4–5 nt loop containing CNGG/CNGGN consensus motifs [66]. We next analyzed the specific sequence within the *FGF2* genome and identified four potential binding sites (BSs), BS137-145, BS260-270, BS743-900, and BS2327-2453. Based on dual luciferase reporter system (Fig. 5a), we detected the two sites, BS137-145 and BS260-270, showing notable reduction in fluorescence intensity in the presence of SAMD4A knockdown (Fig. 5b). Conversely, SAMD4A overexpression induced a substantial increase in expression activity of the two sites (Fig. 5c). Taken together, these outcomes underscored an essential function of SAMD4A in regulating the expression of *FGF2*, in which it can selectively bind to the motifs BS137-145 and BS260-270 within *FGF2* mRNA, thereby modulating translation of the transcripts, which was further confirmed by the alternation of FGF2 protein levels in hESCs upon knockdown (Fig. 5d) or overexpression of SAMD4A (Fig. 5e).

In order to understand whether SAMD4A has impact on *FGF2* mRNA stability, we utilized Actinomycin D to hinder mRNA synthesis (Fig. 5f). Our results revealed that SAMD4A overexpression shielded *FGF2* mRNA from degradation (Fig. 5g). This data implies that SAMD4A has the function to impede the degradation of *FGF2* mRNA for maintaining stable targets.

To ascertain the receptor through which FGF2 exerts its effects, we assessed the mRNA expression of *FGFR1*, *FGFR2*, *FGFR3*, and *FGFR4* in *SAMD4A*-OE-hESCs and *SAMD4A*-KD-hESCs. The expression changes in FGFR2 suggest its role as the receptor for FGF2 (Fig. 5h, i). We next tested the impact of FGFR2 inhibitor (30 μM Formononetin) on *SAMD4A*-overexpressing-hESCs (*SAMD4A*-OE-hESCs) proliferation by qRT-PCR. As expected, we found that FGFR2 inhibitor significantly affected the proliferation markers of *SAMD4A*-OE-hESCs, FGFR2 inhibitor eliminated the increased expression of proliferation markers *KI67*, *AKT1*, *CDK2*, *CDK4*, *CCNB1* in *SAMD4A*-OE-hESCs as shown in Fig. 5j. These results indicate that FGF2 functions through the FGFR2 receptor, stimulating the expression of proliferation markers in *SAMD4A*-OE-hESCs.

SAMD4A mediates FGF2 to drive cardiomyogenesis via the PI3K/AKT/mTOR pathway in hESCs

To detect how SAMD4A mediates cardiomyocyte differentiation, we established a stable *SAMD4A*-overexpressing-hESCs (*SAMD4A*-OE-hESCs) line that steadily overexpressed SAMD4A in hESCs (Supplementary Fig. S8a). Although SAMD4A could be induced 2.5-fold higher (Fig. 6a, b), it has no effect on pluripotency marker genes except for *SOX2* (Fig. 6c, d), indicating a limited role of SAMD4A on pluripotency. However, the proliferation-related marker genes *AKT1*, *CDK4*, *CCNB1*, *CCND1*, and *KI67* were significantly up-regulated, and fluorescence intensity of KI67 also markedly increased (Fig. 6e, f). These results indicated SAMD4A really involved in hESC proliferation.

Next, to assess effects of SAMD4A on the spontaneous differentiation potential of hESCs, we employed the hanging droplet assay to explore the markers alteration at different stages from the three germ layers (ectoderm, endoderm, and mesoderm). The qRT-PCR results revealed the mRNA levels of pluripotency markers *NANOG*, *SOX2*, *OCT4* of EBs on day11 were not influenced, except the expression of *C-MYC* was slightly higher (Supplementary Fig. S8b), and the down regulation was induced in the expression of ectodermal genes *SOX1* and *NESTIN* (Supplementary Fig. S8c), suggesting that SAMD4A may drive hESC differentiation towards the mesoendodermal lineage. Once *SAMD4A*-overexpressing-hESCs (*SAMD4A*-OE-hESCs) were induced to differentiate into cardiomyocyte, many markers accordingly

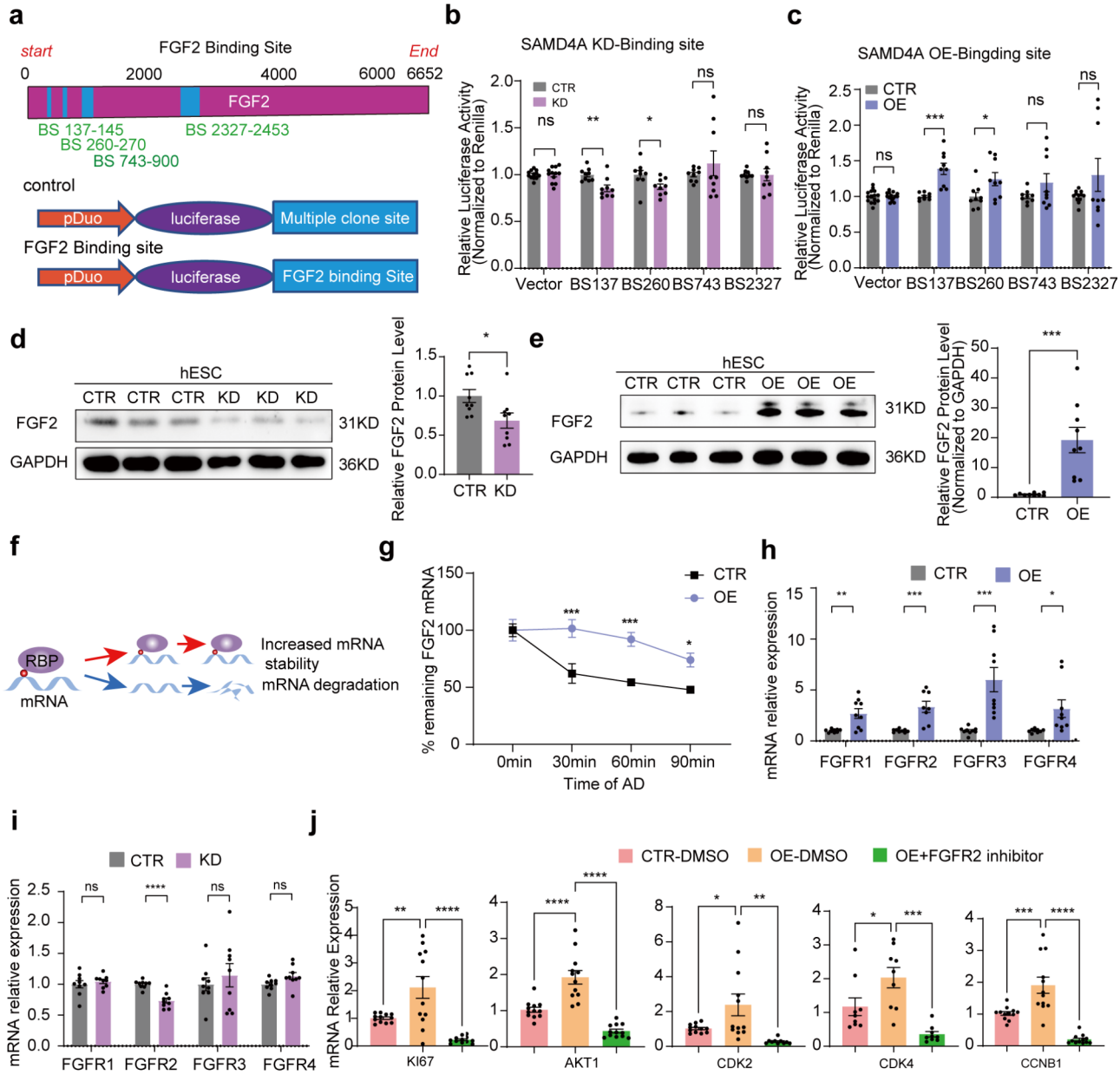

Fig. 5 SAMD4A recognizes specific motifs of the *FGF2* regulating its translation and mRNA stability, while FGFR2 acts as the receptor for *FGF2*. **(a)** The upper panel presented a schematic diagram of the *FGF2* mRNA containing four predicted SAMD4A binding sites: BS137-145, BS260-270, BS743-900, and BS2327-2453. Lower, construction of the dual-luciferase reporter assay with *FGF2* binding sites. **(b)** and **(c)** Quantitative analysis of the relative luciferase reporter activity comparing *SAMD4A* knockdown/overexpression and scramble vector control. The *SAMD4A* knockdown/overexpression plasmid was co-transfected with luciferase reporter plasmids containing FGF2 binding sites for 36 h into HEK293T cells. Firefly luciferase reporter activities were normalized to renilla luciferase reporter activities, with the empty luciferase plasmid co-transfected with the respective *SAMD4A* negative control plasmid acting as the control. **(d)** Western blot demonstrated a significant reduction in the protein levels of FGF2 in *SAMD4A*-knockdown hESCs compared with the respective control. Left, immunoblotting images. Right, statistical analysis of the relative FGF2 protein level normalized to GAPDH. Corresponding uncropped full-length gels and blots are presented in Supplementary Fig. S9. **(e)** Western blot results demonstrated a notable elevation in the protein levels of FGF2 in *SAMD4A*-OE-hESCs compared to the respective control. Left, the immunoblotting image. Right, statistical analysis of the relative FGF2 protein level normalized to GAPDH. Corresponding uncropped full-length gels and blots are presented in Supplementary Fig. S9. **(f)** Schematic illustration depicted the stability of *FGF2* mRNA, which was stable in the presence of SAMD4A protein binding and degraded in the absence of SAMD4A. **(g)***FGF2* mRNA stability assay. Quantification of *FGF2* mRNA abundance in *SAMD4A*-OE-hESCs hESCs after treatment with Actinomycin D (1 μM) at different time points. **(h)** qRT-PCR measured the mRNA expression of *FGF* receptors (*FGFR1*, *FGFR2*, *FGFR3*, *FGFR4*) in *SAMD4A*-OE-hESCs and the scramble control. **(i)** qRT-PCR assessed the mRNA expression of *FGF* receptors (*FGFR1*, *FGFR2*, *FGFR3*, *FGFR4*) in *SAMD4A*-KD-hESCs and the scramble control. **(j)** qRT-PCR illustrated the mRNA expression of proliferation marker genes *KI67*, *AKT1*, *CDK2*, *CDK4*, and *CCNB1*. *SAMD4A*-OE-hESCs and the scramble control hESCs were cultured in FGFR2 inhibitor (30μM Formononetin) and DMSO. **(b)**, **(c)-(e)**, **(h)** and **(i)** Statistical significance was determined by the two-tailed Student's *t*-test. **(g)** and **(j)** Statistical significance was determined by the ordinary one-way ANOVA test. **P* < 0.05, ***P* < 0.01, ****P* < 0.001, and *****P* < 0.0001 vs. control group (mean ± SEM;*n* = 3 from at least three independent experiments)

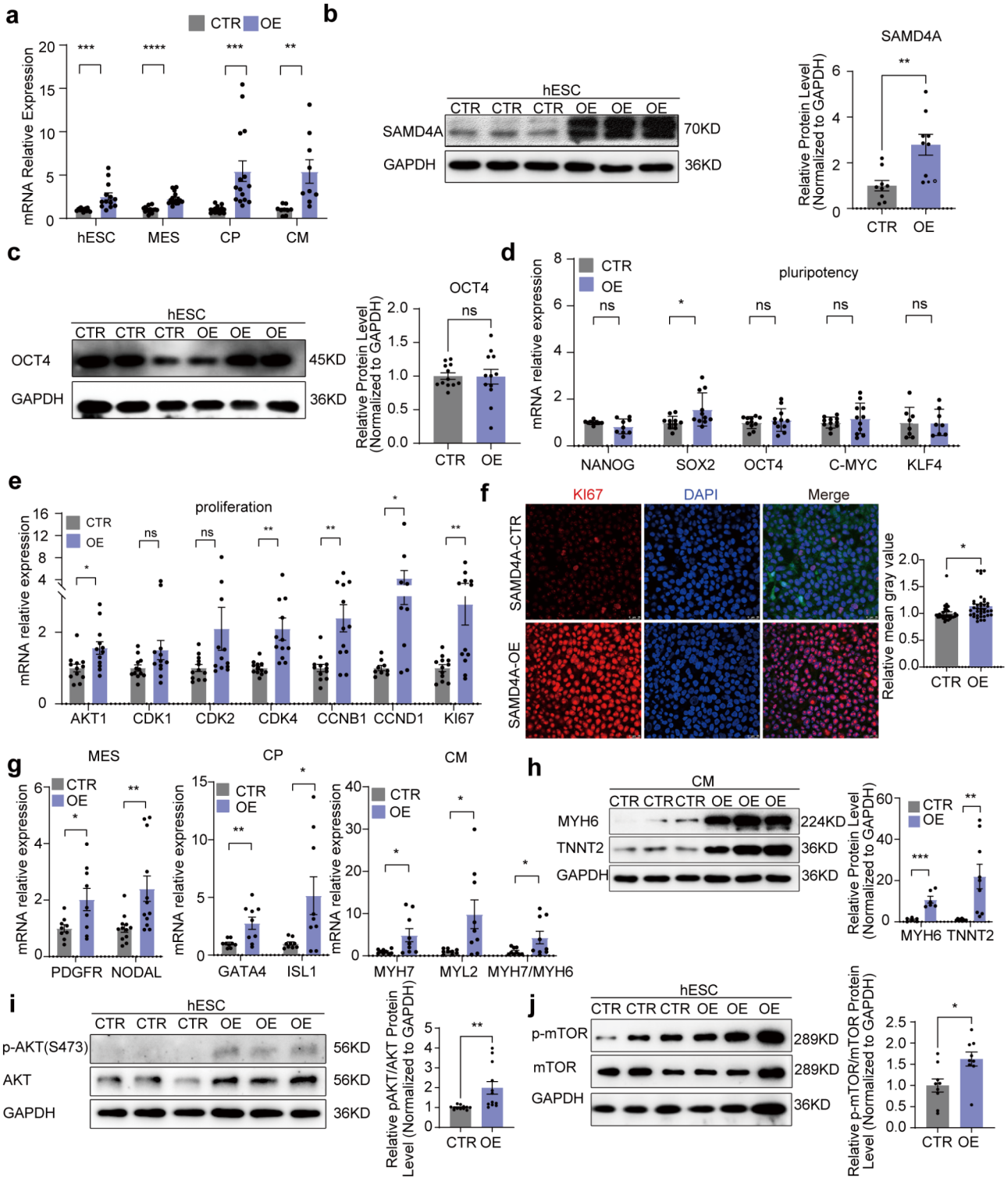

Fig. 6 (See legend on next page.)

(See figure on previous page.)

Fig. 6 Overexpression of SAMD4A in hESCs promotes cardiomyogenesis through mTOR signaling. **(a)** qRT-PCR was conducted to assess the mRNA expression of *SAMD4A* during cardiomyocyte differentiation in *SAMD4A*-OE-hESCs and the corresponding scramble control. **(b)** and **(c)** Western blot revealed a significant increase in the protein levels of SAMD4A and OCT4 in *SAMD4A*-OE-hESCs compared to the respective control. Left, immunoblotting images. Right, statistical analysis of the relative SAMD4A and OCT4 protein levels normalized to GAPDH. Corresponding uncropped full-length gels and blots are presented in Supplementary Fig. S9. **(d)** qRT-PCR was performed to measure the mRNA expression of pluripotency markers (*NANOG*, *SOX2*, *OCT4*, *C-MYC*, *KLF4*) in *SAMD4A*-OE-hESCs and the respective control. **(e)** qRT-PCR analysis assessed the mRNA expression of proliferation markers (*AKT1*, *CDK1*, *CDK2*, *CDK4*, *CCNB1*, *CCND1*, *KI67*) in *SAMD4A*-OE-hESCs and the respective control. **(f)** Immunofluorescence staining of the proliferation marker KI67 in *SAMD4A*-OE-hESCs and the respective control. Left, immunostaining images. Right, relative fluorescence intensity analysis of KI67 in control and *SAMD4A*-OE-hESCs. The both cell-lines inherently express GFP. Scale bars: 25 µm. **(g)** qRT-PCR was utilized to measure the mRNA expression at different time points during cardiomyocyte differentiation in control and *SAMD4A*-OE-hESCs. This included mesoderm-specific genes (*PDGFR*, *NODAL*), cardiac progenitors (*GATA4*, *ISL1*), and cardiomyocyte-specific genes (*MYH7*, *MYL2* with the ratio of *MYH7* to *MYH6* representing a marker of cardiomyocyte maturation). **(h)** Western blot analysis of cardiomyocyte-specific markers (MYH6, TNNT2) was conducted in control and *SAMD4A*-OE-cardiomyocytes. Left, immunoblotting images. Right, relative signal intensity analysis of MYH6 and TNNT2 protein levels, with GAPDH used as a control. Source blots were presented in Supplementary Fig. S9. **(i)** Western blot assessed the relative protein level of AKT and the phosphorylation level of AKT (p-AKT) in *SAMD4A*-OE-hESCs and the respective control compared to GAPDH (left panel). Right, a relative signal intensity analysis of the phosphorylation level of AKT. Corresponding uncropped full-length gels and blots are presented in Supplementary Fig. S9. **(j)** Western blot analysis detected the relative protein level of mTOR and the phosphorylation level of mTOR (p-mTOR) in *SAMD4A*-OE-hESCs and the respective control compared to GAPDH (left panel). Right, a quantitative analysis of the phosphorylation level of mTOR. Corresponding uncropped full-length gels and blots are presented in Supplementary Fig. S9. Statistical significance was analysed by the two-tailed Student's *t*-test, indicating significant differences with $^{*}P < 0.05$, $^{**}P < 0.01$, $^{***}P < 0.001$, and $^{****}P < 0.0001$ vs. control group (mean ± SEM;$n = 3$ from at least three independent experiments)

shown up-regulation in expression, including mesoderm marker genes *PDGFR* and *NODAL*, cardiac progenitor markers *GATA4* and *ISL1*, as well as cardiac-specific genes *MYH7* and *MYL2*. Moreover, the *MYH7/MYH6* ratio was increased to the benefit of cardiomyocyte maturation (Fig. 6g). In addition, *SAMD4A*-OE mesoderm cells exhibited a remarkable increase in the mRNA level of mesoendoderm markers (*FOXA2*, *SOX17*, and *PITX2*), while the marker genes for ectoderm, such as OTX2, decreased significantly (Supplementary Fig. S8d). The protein levels of MYH6 and TNNT2 were also significantly elevated (Fig. 6h) and the beating rates increased significantly (Supplementary Fig. S8e, Supplementary Videos S3, S4). Furthermore, genes associated with cardiomyocyte contractile function, including *NEBL* and *PDLIM5*, as well as calcium regulatory genes such as *SERCA2*, *CAMK2D*, and *CALM2* exhibited upregulation in *SAMD4A*-OE-CMs, as validated by qPCR (Supplementary Fig. S8f).

Additionally, SAMD4A upregulation promoted the phosphorylation of AKT and mTOR that was necessary to activate the pathway (Fig. 6i, j). Therefore, these findings collectively indicate that SAMD4A can bind with *FGF2* to modulate hESC-derived cardiomyocytes through mediating PI3K/AKT/mTOR signalling.

Discussion

The RBP SAMD4A exhibits high expression levels during the embryonic development of the heart, spanning from post-conception 4 weeks (4pcw) to toddlerhood, suggesting a potential role in the process. However, the precise physiological effect and molecular mechanisms underlying SAMD4A's involvement in embryonic heart development remain unclear. In this study, we generated hESC lines with SAMD4A knockdown or overexpression, revealing SAMD4A as a significant regulator in cardiomyocyte lineage commitment.

Despite SAMD4A knockdown did not alter normal stem cell morphology and general feature, *SOX2* and *NANOG* were obviously down-regulated, along with an inhibition of proliferation marker genes such as *AKT1*, *CDK2*, *CDK4*, *CCNB1*, and *KI67*. *NANOG*, *OCT4*, and *SOX2* collectively coordinated proliferation and pluripotency of hESCs [67]. Notably, these pluripotency genes not only regulate pluripotency but also influence specific cell differentiation fates [68]. Our results show that SAMD4A knockdown inhibits proliferation marker genes and reduces cardiac-specific mesodermal markers. RNA-seq analysis revealed that DEGs were enriched in cardiomyocyte lineage differentiation pathways, specifically PI3K/AKT/mTOR pathway, suggesting that SAMD4A plays a dual role in regulating both stem cell proliferation and cardiomyocyte differentiation.

Mammalian Samd4a directly binds to RNA molecules to act its function as a translation repressor. In Drosophila, homolog Smaug inhibits the translation via hindering assembly of translation initiation complexes [32, 69]. However, human SAMD4A exhibits a dual role, functioning both as an inhibitor and promoter in translation [29, 70]. In this work, by employing a bioinformatics tool to analyze SAMD4A's target mRNAs and further intersecting this prediction with our own RNA-seq data, we identified *FGF2* mRNA as a potential binding target for SAMD4A. Even though the FGF signaling axis has been suggested to be crucial in cardiac development, the underlying molecular details remain unclear [71–74].

Our results demonstrate a positive regulatory relationship between SAMD4A and FGF2 expression, and functionally establish FGF2 as the pivotal mediator through which SAMD4A governs the PI3K/AKT/mTOR pathway. RBPs possess distinct structural domains, influencing various biological processes through specific binding motif preferences [75, 76]. Additionally, we confirmed

again that SAMD4A indeed specifically recognizes a short loop containing the CNGG/CNGGN motif [66], in which we identified four potential binding sites on *FGF2* mRNA. SAMD4A primarily influences the translation of *FGF2* mRNA through binding with the BS137-145 and BS260-270 motifs. Furthermore, our results demonstrate that SAMD4A impedes the degradation of *FGF2* mRNA, suggesting that the RBP promotes *FGF2* translation via maintaining its mRNA stability. Therefore, SAMD4A can target to specific mRNAs to exert multiple functions in controlling the expression of distinct genes involved in various biological processes.

The FGF relies on the PI3K/AKT pathway mediated by FRS2α to regulate mTOR [77] in both in vivo and in vitro cardiomyogenesis. As a pivotal developmental regulator, FGF participates in signal transduction cascades via receptor tyrosine kinases (RTKs), prominently activating the PI3K/AKT/mTOR and ERK1/2 pathways. However, it remains elusive whether FGF operates exclusively through its primary signal transduction cascade [78]. The intricate crosstalk among these signaling, potentially influence of the SAMD4A on other signaling cascades, collectively participates in cell fate decision. Nevertheless, a comprehensive understanding in cardiomyocytes differentiation remains further clarified.

Conclusion

In conclusion, we found that SAMD4A mediated *FGF2* for the activation of distinct SAMD4A-dependent *FGF2* downstream signaling pathways, particularly the FGF2-FGFR2-PI3K/AKT/mTOR signaling axis, playing coordinating role for stem cell proliferation and lineage specification. This activation either maintains ESCs in a pluripotent stage or promotes the progression of cardiomyogenesis. Therefore, our study offers unknown insights into the function of RBPs in the processes of heart development and cardiomyogenesis.

Study limitations

Here, we have reported the specific role of SAMD4A in stem cell self-renewal and cardiomyocyte lineage specification targeting *FGF2* through PI3K/AKT/mTOR pathway. This study has several limitations. Firstly, although SAMD4A is critical for hESC cell fate decisions, further systematic investigations are needed to elucidate its potential regulatory role in cardiomyocytes function and maturation, particularly with regard to its influence on cardiomyocyte electrophysiology, calcium handling, and metabolism. Secondly, it is essential to recognize the substantial differences between in vitro and in vivo conditions for cardiomyocyte differentiation. The in vivo microenvironment of the developing human embryonic heart is intricately regulated by multiple factors and signaling pathways [1–4], making it challenging to fully replicate this environment in vitro, which may limit the study's findings. Further validation through 3D cardiac organoid models or in vivo experiments in animals is needed. Additionally, while SAMD4A, as an RBP, binds specific mRNAs, the identification of additional targets and the precise mechanisms through which it exerts its effects remain to be determined. Here, we provide evidence highlighting the functional importance of SAMD4A in cardiomyocyte differentiation, emphasizing the need for future studies to explore the potential role of SAMD4A misregulation in CHDs.

Abbreviations

RBPs	RNA-binding proteins
DEGs	Differentially expressed genes
TFs	Transcription factors
CHD	Congenital heart disease
SAM	Sterile alpha motif
shRNA	A small hairpin RNA or short hairpin RNA
SAMD4A-CTR-hESCs	SAMD4A-control-hESCs
SAMD4A-KD-hESCs	SAMD4A-knockdown-hESCs
SAMD4A-OE-hESCs	SAMD4A-overexpressing-hESCs
qRT-PCR	Real-time quantitative Polymerase Chain Reaction
FDR	False discovery rate
GSEA	Gene set enrichment analysis
GO	Gene Ontology
KEGG	Kyoto Encyclopedia of Genes and Genomes
RIP	RNA immunoprecipitation
BS	Binding site
LUC	Luciferase

Supplementary Information

The online version contains supplementary material available at https://doi.org/10.1186/s13287-025-04269-7.

Supplementary Material 1: Uncropped WB membranes. Full-length blots.

Supplementary Material 2: Fig. S1. Model of the hESC-derived CMs and characterization of the SAMD4A knockdown effects. **Fig. S2.** Expression of Samd4a in the mESC-derived CMs model and during early mouse development. **Fig. S3.** The expression patterns of SAMD4A in various cell types within human heart samples. **Fig. S4.** Reduction of SAMD4A induced lineage commitment to differentiation of three germ layers and SAMD4A is required for the appropriate differentiation of human cardiomyocytes. **Fig. S5.** SAMD4A is required for the cardiac differentiation. **Fig. S6.** RIP-qPCR analysis to confirm the potential targets of RNA binding protein SAMD4A. **Fig. S7.** Functions of SAMD4A by targeting FGF2. **Fig. S8.** Characterization of the SAMD4A after overexpression in hESCs.

Supplementary Material 3: Video S1. Beating SAMD4A-CTR cardiomyocytes on differentiation day 15, related to Figure S4d.

Supplementary Material 4: Video S2. Beating SAMD4A-KD cardiomyocytes on differentiation day 15, related to Figure S4d.

Supplementary Material 5: Video S3. Beating SAMD4A-CTR cardiomyocytes on differentiation day 15, related to Figure S8e.

Supplementary Material 6: Video S4. Beating SAMD4A-OE cardiomyocytes on differentiation day 15, related to Figure S8e.

Supplementary Material 7: Table S1. The primers used for PCR/qPCR assays and the antibodies and reagents employed in this study.

Supplementary Material 8: Table S2. Differentially expressed genes (DEGs) of down-regulation in knockdown SAMD4A hESCs relative to wild-type hESCs.

Acknowledgements
We thank Prof. Qing Jing from Shanghai Institutes for Biological Sciences Chinese Academy of Sciences for the kindly donation of human ESC line WA07 (H7) used in this study, and their hESC line WA07 (H7) was obtained from WiCell (Madison, WI).

Author contributions
NY and LL conceived the project and designed the experiments; NY and HRW performed the major experiments and data analysis, manuscript writing; YPZ, YZS, and HL performed the plasmid construction and other experiments; QL and TX helped with the RNA-seq data analysis; YLM, FL, SYH, HMC, and JFZ contributed to paper writing and review of the manuscript; LYP and LL revised the manuscript. All authors read and discussed the manuscript.

Funding
This research was supported by the National Natural Science Foundation of China (82070270, 82470408), the Shanghai Committee of Science and Technology (22ZR1463800), Li Li is a fellow at the Collaborative Innovation Center for Cardiovascular Disease Translational Medicine, Nanjing Medical University.

Data availability
RNA-seq data in this study generated have been available on the Gene Expression Omnibus database under (GSE255152), further detail of the data and materials in this paper are available to require directly from corresponding authors.

Declarations

Ethics approval and consent to participate
Human ESC line WA07 (H7) used in this study was kindly donated by Prof. Qing Jing from Shanghai Institutes for Biological Sciences Chinese Academy of Sciences. Their hESC line (H7) was obtained from WiCell (Madison, WI) (WA07). The use of the hESC line was approved by the Ethical Committee of Changhai Hospital, and the original publication on the cell line by the source lab is cited in reference 36 (PMID: 28971953).

Consent for publication
All authors confirm their consent for publication.

Artificial intelligence
The authors declare that artificial intelligence is not used in this study.

Competing interests
All authors certify that they have no conflicts of interest.

Received: 15 October 2024 / Accepted: 6 March 2025
Published online: 18 March 2025

References

1. Meilhac SM, Buckingham ME. The deployment of cell lineages that form the mammalian heart. Nat Rev Cardiol. 2018;15:705–24.
2. Paige SL, Plonowska K, Xu A, Wu SM. Molecular regulation of cardiomyocyte differentiation. Circ Res. 2015;116:341–53.
3. Burridge PW, Sharma A, Wu JC. Genetic and epigenetic regulation of human cardiac reprogramming and differentiation in regenerative medicine. Annu Rev Genet. 2015;49:461–84.
4. de Bruin RG, Rabelink TJ, van Zonneveld AJ, van der Veer EP. Emerging roles for RNA-binding proteins as effectors and regulators of cardiovascular disease. Eur Heart J. 2017;38:1380–8.
5. Nees SN, Chung WK. Genetic basis of human congenital heart disease. Cold Spring Harb Perspect Biol. 2020;12.
6. Zaidi S, Brueckner M. Genetics and genomics of congenital heart disease. Circ Res. 2017;120:923–40.
7. van der Linde D, Konings EE, Slager MA, Witsenburg M, Helbing WA, Takkenberg JJ, Roos-Hesselink JW. Birth prevalence of congenital heart disease worldwide: a systematic review and meta-analysis. J Am Coll Cardiol. 2011;58:2241–7.
8. Mozaffarian D, Benjamin EJ, Go AS, Arnett DK, Blaha MJ, Cushman M, de Ferranti S, Despres JP, Fullerton HJ, Howard VJ, et al. Heart disease and stroke statistics–2015 update: a report from the American heart association. Circulation. 2015;131:e29–322.
9. Roth GA, Mensah GA, Johnson CO, Addolorato G, Ammirati E, Baddour LM, Barengo NC, Beaton AZ, Benjamin EJ, Benziger CP, et al. Global burden of cardiovascular diseases and risk factors, 1990–2019: update from the GBD 2019 study. J Am Coll Cardiol. 2020;76:2982–3021.
10. Blech-Hermoni Y, Ladd AN. RNA binding proteins in the regulation of heart development. Int J Biochem Cell Biol. 2013;45:2467–78.
11. Ye J, Blelloch R. Regulation of pluripotency by RNA binding proteins. Cell Stem Cell. 2014;15:271–80.
12. Lu Y, Loh YH, Li H, Cesana M, Ficarro SB, Parikh JR, Salomonis N, Toh CX, Andreadis ST, Luckey CJ, et al. Alternative splicing of MBD2 supports self-renewal in human pluripotent stem cells. Cell Stem Cell. 2014;15:92–101.
13. Lu X, Goke J, Sachs F, Jacques PE, Liang H, Feng B, Bourque G, Bubulya PA, Ng HH. SON connects the splicing-regulatory network with pluripotency in human embryonic stem cells. Nat Cell Biol. 2013;15:1141–52.
14. Han H, Irimia M, Ross PJ, Sung HK, Alipanahi B, David L, Golipour A, Gabut M, Michael IP, Nachman EN, et al. MBNL proteins repress ES-cell-specific alternative splicing and reprogramming. Nature. 2013;498:241–5.
15. Lackford B, Yao C, Charles GM, Weng L, Zheng X, Choi EA, Xie X, Wan J, Xing Y, Freudenberg JM, et al. Fip1 regulates mRNA alternative polyadenylation to promote stem cell self-renewal. EMBO J. 2014;33:878–89.
16. Frye M, Harada BT, Behm M, He C. RNA modifications modulate gene expression during development. Science. 2018;361:1346–9.
17. Jao LE, Appel B, Wente SR. A zebrafish model of lethal congenital contracture syndrome 1 reveals Gle1 function in spinal neural precursor survival and motor axon arborization. Development. 2012;139:1316–26.
18. Ramanathan A, Robb GB, Chan SH. mRNA capping: biological functions and applications. Nucleic Acids Res. 2016;44:7511–26.
19. Stowell JAW, Webster MW, Kogel A, Wolf J, Shelley KL, Passmore LA. Reconstitution of targeted deadenylation by the Ccr4-Not complex and the YTH domain protein Mmi1. Cell Rep. 2016;17:1978–89.
20. Viswanathan SR, Daley GQ, Gregory RI. Selective Blockade of MicroRNA processing by Lin28. Science. 2008;320:97–100.
21. Rigaud VOC, Hoy RC, Kurian J, Zarka C, Behanan M, Brosious I, Pennise J, Patel T, Wang T, Johnson J, et al. RNA-Binding protein LIN28a regulates new myocyte formation in the heart through long noncoding RNA-H19. Circulation. 2023;147:324–37.
22. Montanes-Agudo P, Aufiero S, Schepers EN, van der Made I, Cocera-Ortega L, Ernault AC, Richard S, Kuster DWD, Christoffels VM, Pinto YM, et al. The RNA-binding protein QKI governs a muscle-specific alternative splicing program that shapes the contractile function of cardiomyocytes. Cardiovasc Res. 2023;119:1161–74.
23. Chen X, Liu Y, Xu C, Ba L, Liu Z, Li X, Huang J, Simpson E, Gao H, Cao D, et al. QKI is a critical pre-mRNA alternative splicing regulator of cardiac myofibrillogenesis and contractile function. Nat Commun. 2021;12:89.
24. Verma SK, Deshmukh V, Thatcher K, Belanger KK, Rhyner AM, Meng S, Holcomb RJ, Bressan M, Martin JF, Cooke JP, et al. RBFOX2 is required for Establishing RNA regulatory networks essential for heart development. Nucleic Acids Res. 2022;50:2270–86.
25. Wang Y, Yi N, Hu Y, Zhou X, Jiang H, Lin Q, Chen R, Liu H, Gu Y, Tong C, et al. Molecular signatures and networks of cardiomyocyte differentiation in humans and mice. Mol Ther Nucleic Acids. 2020;21:696–711.
26. Volkers M, Preiss T, Hentze MW. RNA-binding proteins in cardiovascular biology and disease: the beat goes on. Nat Rev Cardiol. 2024;21:361–78.
27. Hill MC, Kadow ZA, Long H, Morikawa Y, Martin TJ, Birks EJ, Campbell KS, Nerbonne J, Lavine K, Wadhwa L, et al. Integrated multi-omic characterization of congenital heart disease. Nature. 2022;608:181–91.
28. Chen L, Dumelie JG, Li X, Cheng MH, Yang Z, Laver JD, Siddiqui NU, Westwood JT, Morris Q, Lipshitz HD, et al. Global regulation of mRNA translation and stability in the early Drosophila embryo by the Smaug RNA-binding protein. Genome Biol. 2014;15:R4.
29. de Haro M, Al-Ramahi I, Jones KR, Holth JK, Timchenko LT, Botas J. Smaug/SAMD4A restores translational activity of CUGBP1 and suppresses CUG-induced myopathy. PLoS Genet. 2013;9:e1003445.
30. Pinder BD, Smibert CA. microRNA-independent recruitment of argonaute 1 to nanos mRNA through the Smaug RNA-binding protein. EMBO Rep. 2013;14:80–6.
31. Zaessinger S, Busseau I, Simonelig M. Oskar allows nanos mRNA translation in Drosophila embryos by preventing its deadenylation by Smaug/CCR4. Development. 2006;133:4573–83.
32. Nelson MR, Leidal AM, Smibert CA. Drosophila cup is an eIF4E-binding protein that functions in Smaug-mediated translational repression. EMBO J. 2004;23:150–9.

33. Gingras AC, Raught B, Sonenberg N. eIF4 initiation factors: effectors of mRNA recruitment to ribosomes and regulators of translation. Annu Rev Biochem. 1999;68:913–63.
34. Chen Z, Holland W, Shelton JM, Ali A, Zhan X, Won S, Tomisato W, Liu C, Li X, Moresco EM, et al. Mutation of mouse Samd4 causes leanness, myopathy, uncoupled mitochondrial respiration, and dysregulated mTORC1 signaling. Proc Natl Acad Sci U S A. 2014;111:7367–72.
35. Niu N, Xiang JF, Yang Q, Wang L, Wei Z, Chen LL, Yang L, Zou W. RNA-binding protein SAMD4 regulates skeleton development through translational Inhibition of Mig6 expression. Cell Discov. 2017;3:16050.
36. Qiu XX, Liu Y, Zhang YF, Guan YN, Jia QQ, Wang C, Liang H, Li YQ, Yang HT, Qin YW et al. Rapamycin and CHIR99021 coordinate robust cardiomyocyte differentiation from human pluripotent stem cells via reducing p53-Dependent apoptosis. J Am Heart Assoc. 2017;6.
37. Ueno S, Weidinger G, Osugi T, Kohn AD, Golob JL, Pabon L, Reinecke H, Moon RT, Murry CE. Biphasic role for Wnt/beta-catenin signaling in cardiac specification in zebrafish and embryonic stem cells. Proc Natl Acad Sci U S A. 2007;104:9685–90.
38. Itskovitz-Eldor J, Schuldiner M, Karsenti D, Eden A, Yanuka O, Amit M, Soreq H, Benvenisty N. Differentiation of human embryonic stem cells into embryoid bodies compromising the three embryonic germ layers. Mol Med. 2000;6:88–95.
39. Huang X, Wu SM. Isolation and functional characterization of pluripotent stem cell-derived cardiac progenitor cells. Curr Protoc Stem Cell Biol. 2010;Chap. 1:Unit 1F 10.
40. A EM. Isolation and propagation of mouse embryonic fibroblasts and Preparation of mouse embryonic feeder layer cells. Curr Protoc Stem Cell Biol. 2007;Chap. 1:Unit1C 3.
41. Kim D, Langmead B, Salzberg SL. HISAT: a fast spliced aligner with low memory requirements. Nat Methods. 2015;12:357–60.
42. Anders S, Pyl PT, Huber W. HTSeq–a Python framework to work with high-throughput sequencing data. Bioinformatics. 2015;31:166–9.
43. Love MI, Huber W, Anders S. Moderated Estimation of fold change and dispersion for RNA-seq data with DESeq2. Genome Biol. 2014;15:550.
44. Benjamini Y, Drai D, Elmer G, Kafkafi N, Golani I. Controlling the false discovery rate in behavior genetics research. Behav Brain Res. 2001;125:279–84.
45. Ashburner M, Ball CA, Blake JA, Botstein D, Butler H, Cherry JM, Davis AP, Dolinski K, Dwight SS, Eppig JT, et al. Gene ontology: tool for the unification of biology. The gene ontology consortium. Nat Genet. 2000;25:25–9.
46. Draghici S, Khatri P, Tarca AL, Amin K, Done A, Voichita C, Georgescu C, Romero R. A systems biology approach for pathway level analysis. Genome Res. 2007;17:1537–45.
47. Korsunsky I, Millard N, Fan J, Slowikowski K, Zhang F, Wei K, Baglaenko Y, Brenner M, Loh PR, Raychaudhuri S. Fast, sensitive and accurate integration of single-cell data with harmony. Nat Methods. 2019;16:1289–96.
48. Li L, Tao G, Hill MC, Zhang M, Morikawa Y, Martin JF. Pitx2 maintains mitochondrial function during regeneration to prevent myocardial fat deposition. Development. 2018;145.
49. Gorski PA, Kho C, Oh JG. Measuring cardiomyocyte contractility and calcium handling in vitro. Methods Mol Biol. 2018;1816:93–104.
50. Litvinukova M, Talavera-Lopez C, Maatz H, Reichart D, Worth CL, Lindberg EL, Kanda M, Polanski K, Heinig M, Lee M, et al. Cells of the adult human heart. Nature. 2020;588:466–72.
51. Garay BI, Givens S, Abreu P, Liu M, Yucel D, Baik J, Stanis N, Rothermel TM, Magli A, Abrahante JE, et al. Dual Inhibition of MAPK and PI3K/AKT pathways enhances maturation of human iPSC-derived cardiomyocytes. Stem Cell Rep. 2022;17:2005–22.
52. Ghigo A, Laffargue M, Li M, Hirsch E. PI3K and calcium signaling in cardiovascular disease. Circ Res. 2017;121:282–92.
53. Dewenter M, von der Lieth A, Katus HA, Backs J. Calcium signaling and transcriptional regulation in cardiomyocytes. Circ Res. 2017;121:1000–20.
54. Jeyaraj SC, Unger NT, Chotani MA. Rap1 GTPases: an emerging role in the cardiovasculature. Life Sci. 2011;88:645–52.
55. Armaos A, Colantoni A, Proietti G, Rupert J, Tartaglia GG. CatRAPID omics v2.0: going deeper and wider in the prediction of protein-RNA interactions. Nucleic Acids Res. 2021;49:W72–9.
56. Vallier L, Alexander M, Pedersen RA. Activin/Nodal and FGF pathways cooperate to maintain pluripotency of human embryonic stem cells. J Cell Sci. 2005;118:4495–509.
57. Sugi Y, Sasse J, Lough J. Inhibition of precardiac mesoderm cell proliferation by antisense oligodeoxynucleotide complementary to fibroblast growth factor-2 (FGF-2). Dev Biol. 1993;157:28–37.
58. Sugi Y, Lough J. Activin-A and FGF-2 mimic the inductive effects of anterior endoderm on terminal cardiac myogenesis in vitro. Dev Biol. 1995;168:567–74.
59. Solloway MJ, Harvey RP. Molecular pathways in myocardial development: a stem cell perspective. Cardiovasc Res. 2003;58:264–77.
60. Brewer JR, Molotkov A, Mazot P, Hoch RV, Soriano P. Fgfr1 regulates development through the combinatorial use of signaling proteins. Genes Dev. 2015;29:1863–74.
61. Watanabe S, Umehara H, Murayama K, Okabe M, Kimura T, Nakano T. Activation of Akt signaling is sufficient to maintain pluripotency in mouse and primate embryonic stem cells. Oncogene. 2006;25:2697–707.
62. Zhou J, Su P, Wang L, Chen J, Zimmermann M, Genbacev O, Afonja O, Horne MC, Tanaka T, Duan E, et al. mTOR supports long-term self-renewal and suppresses mesoderm and endoderm activities of human embryonic stem cells. Proc Natl Acad Sci U S A. 2009;106:7840–5.
63. Armstrong L, Hughes O, Yung S, Hyslop L, Stewart R, Wappler I, Peters H, Walter T, Stojkovic P, Evans J, et al. The role of PI3K/AKT, MAPK/ERK and NFkappabeta signalling in the maintenance of human embryonic stem cell pluripotency and viability highlighted by transcriptional profiling and functional analysis. Hum Mol Genet. 2006;15:1894–913.
64. Ludwig TE, Bergendahl V, Levenstein ME, Yu J, Probasco MD, Thomson JA. Feeder-independent culture of human embryonic stem cells. Nat Methods. 2006;3:637–46.
65. Craig A, Smibert JEW, Kerr K. Macdonald. smaug protein represses translation of unlocalized nanos mRNA in the Drosophila embryo. GENES& DEVELOPMEN. 1996;10:2600–9.
66. Aviv T, Lin Z, Lau S, Rendl LM, Sicheri F, Smibert CA. The RNA-binding SAM domain of Smaug defines a new family of post-transcriptional regulators. Nat Struct Biol. 2003;10:614–21.
67. Ng HH, Surani MA. The transcriptional and signalling networks of pluripotency. Nat Cell Biol. 2011;13:490–6.
68. Wang Z, Oron E, Nelson B, Razis S, Ivanova N. Distinct lineage specification roles for NANOG, OCT4, and SOX2 in human embryonic stem cells. Cell Stem Cell. 2012;10:440–54.
69. Jeske M, Moritz B, Anders A, Wahle E. Smaug assembles an ATP-dependent stable complex repressing nanos mRNA translation at multiple levels. EMBO J. 2011;30:90–103.
70. Baez MV, Boccaccio GL. Mammalian Smaug is a translational repressor that forms cytoplasmic foci similar to stress granules. J Biol Chem. 2005;280:43131–40.
71. Zhang J, Liu J, Huang Y, Chang JY, Liu L, McKeehan WL, Martin JF, Wang F. FRS2alpha-mediated FGF signals suppress premature differentiation of cardiac stem cells through regulating autophagy activity. Circ Res. 2012;110:e29–39.
72. Frank DU, Fotheringham LK, Brewer JA, Muglia LJ, Tristani-Firouzi M, Capecchi MR, Moon AM. An Fgf8 mouse mutant phenocopies human 22q11 deletion syndrome. Development. 2002;129:4591–603.
73. Park EJ, Watanabe Y, Smyth G, Miyagawa-Tomita S, Meyers E, Klingensmith J, Camenisch T, Buckingham M, Moon AM. An FGF autocrine loop initiated in second heart field mesoderm regulates morphogenesis at the arterial pole of the heart. Development. 2008;135:3599–610.
74. Zhang J, Lin Y, Zhang Y, Lan Y, Lin C, Moon AM, Schwartz RJ, Martin JF, Wang F. Frs2alpha-deficiency in cardiac progenitors disrupts a subset of FGF signals required for outflow tract morphogenesis. Development. 2008;135:3611–22.
75. Lunde BM, Moore C, Varani G. RNA-binding proteins: modular design for efficient function. Nat Rev Mol Cell Biol. 2007;8:479–90.
76. Ray D, Kazan H, Chan ET, Pena Castillo L, Chaudhry S, Talukder S, Blencowe BJ, Morris Q, Hughes TR. Rapid and systematic analysis of the RNA recognition specificities of RNA-binding proteins. Nat Biotechnol. 2009;27:667–70.
77. Lin X, Zhang Y, Liu L, McKeehan WL, Shen Y, Song S, Wang F. FRS2alpha is essential for the fibroblast growth factor to regulate the mTOR pathway and autophagy in mouse embryonic fibroblasts. Int J Biol Sci. 2011;7:1114–21.
78. Ray AT, Mazot P, Brewer JR, Catela C, Dinsmore CJ, Soriano P. FGF signaling regulates development by processes beyond canonical pathways. Genes Dev. 2020;34:1735–52.

Publisher's note